THESIS

IMAGING THE LITHOSPHERE OF WESTERN CANADA WITH AMBIENT NOISE DATA

Submitted by

Tomalika Biswas

Department of Geosciences

In partial fulfillment of the requirements

For the Degree of Master of Science

Colorado State University

Fort Collins, Colorado

Summer 2026

Master's Committee:

Advisor: Derek Schutt

Rick Aster
Kristen Buchanan

ABSTRACT

IMAGING THE LITHOSPHERE OF WESTERN CANADA WITH AMBIENT NOISE DATA

The Canadian Cordillera represents a key transition zone from the present-day Pacific plate boundary, through the tectonically active Phanerozoic Cordilleran orogen, to the stable Precambrian craton of North America. This thesis uses ambient noise tomography to image the geometry of lithosphere across the Cordillera-craton transition with improved spatial resolution. More than six thousand day-long vertical-component seismic waveforms from over one hundred broadband seismic stations were analyzed across western Canada. Rayleigh wave phase velocity maps were generated for periods from 6.0 to 60.0 s. These maps were supported by uncertainty estimates, velocity perturbation maps, and inversion convergence results. The period-dependent phase velocity information was further used to develop shear wave velocity (Vs) depth slices at 10, 20, 30, 40, and 50 km depth.

The results show strong lateral velocity variations across western Canada. At shorter periods, the phase velocity maps mainly reflect shallow crustal heterogeneity, including sedimentary basin effects and upper-crustal variations. At intermediate and longer periods, the contrast between the Cordillera and the craton becomes more pronounced. The Vs depth slices further show that this contrast strengthens with depth. Low Vs values beneath the Cordillera indicate warmer, thinner, and more deformed lithosphere, whereas high Vs values beneath the craton reflect colder, thicker, and more stable lithospheric mantle. Overall, this study provides higher-resolution seismic images of the lithosphere beneath western Canada through Rayleigh wave phase velocity maps and Vs depth slices. The result of the study area helps constrain the geometry of the lithospheric transition and provides a basis for future studies integrating seismic, thermal, and tectonic observations across western Canada.

ACKNOWLEDGEMENTS

I would like to thank my advisor, Dr. Derek Schutt, for his invaluable support and guidance throughout my educational journey here at CSU. I would also like to thank all the faculty members at the Department of Geosciences at CSU for teaching such intellectually stimulating courses and allowing me to be a Teaching Assistant. A big thank you to my family for their love and support (both emotional and financial). Lastly, special thanks to Dr. Jeremy Gosselin, the writer of the "ambient noise tomography" code used in this study, for his guidance on its execution.

LIST OF CONTENTS

LIST OF FIGURES

Chapter 1

Introduction and Framework

1.1 Introduction

This master's thesis comprises four chapters detailing the lithospheric characteristics of Western Canada through ambient noise tomography.

Chapter One establishes the project's foundational background, describing the essentials of ambient noise tomography and processing concepts. It provides an overview of the theoretical frameworks and methodologies supporting the research, setting the stage for more intricate analyses.

Chapter Two outlines the tectonic and geological setting of western Canada, emphasizing the contrast between the stable North American craton and the active Canadian Cordillera. It describes major structural features such as the Rocky Mountain Trench and Tintina Fault and reviews gaps in previous geophysical research. The chapter also details the data selection and processing workflow, including preprocessing, cross-correlation, stacking, and cleaning that is used to generate phase velocity maps for the tomographic inversion.

Chapter Three describes the results and discussion of the study. It includes phase velocity maps, uncertainty maps, velocity perturbation maps, shear wave velocity depth slices, and inversion convergence results. The interpretation focuses on the major velocity contrast between the tectonically active Cordillera and the stable craton. The chapter also discusses how this velocity patterns relate to lithospheric structure, crustal heterogeneity, tectonic setting, and geological variation across western Canada.

Chapter Four explores potential directions for future research, focusing on advancements in ambient noise tomography, improved data integration, and higher-resolution seismic imaging. This chapter discusses methodological improvements, additional data sources, and how the results can be expanded upon to further investigate the lithospheric structure of Western Canada.

Overall, this thesis aims to contribute to the understanding of lithospheric structure beneath western Canada. By utilizing ambient noise tomography, this study provides new insight into the crust and uppermost mantle, particularly the transition between the Cordillera and the craton. The results also provide a useful framework for future studies of lithospheric geometry and tectonic evolution in this region.

1.2 Background

Western Canada is a geologically complex and diverse region that includes British Columbia, Alberta, Saskatchewan, Manitoba, Yukon, and the Northwest Territories. It contains various crustal blocks, accreted terranes, fault systems, and lithospheric thickness and temperature variations, representing a tectonic evolution that spans billions of years of Earth's history. This region provides an ideal environment for studying continental accretion, growth processes, structure variations, geometry variations, and the upper surface's physical properties from the Archaean to the present day. The ancient core of the North American continent consists of several Archean provinces that form part of one of the oldest continental cratons in the world. Following the collision of these former "microcontinents" to form the ancestral core, the North American continent was expanded by the Paleoproterozoic accretion of several distinct oceanic terranes. The most recent significant period of westward expansion began in the Phanerozoic, which resulted in the accretion of much of the present-day crust of the Canadian Cordillera (Hoffman, 1988; Ross et al., 1991; Sears et al., 2007).

The western margin of Canada also provides an opportunity to study the complex transition from the convergent boundary to the transform boundary [Figure 5.1]. This region is dominated by continuous tectonic activity, with the subduction of the Juan de Fuca plate beneath the North American plate in the south and the transform motion of the Pacific plate along the Queen Charlotte Fault in the north. Subduction of the Juan de Fuca plate is an active process, generating compressional forces that result in crustal deformation, mountain building, and seismic activity. However, further north, this subduction transitions into a strike-slip (transform) boundary, where the Pacific plate moves laterally past the North American plate along the Queen Charlotte Fault. This transition from convergent subduction to strike-slip motion creates a complex tectonic environment characterized by a mix of compressional and extensional forces across the region. The Queen Charlotte Fault, running offshore parallel to the western coastline of British Columbia, defines this transform boundary and accommodates lateral plate motion, leading to seismic activity and crustal deformation. The resulting interplay between subduction-related compression in the south and strike-slip motion in the north influences the structural evolution and geodynamics of Western Canada.

Further north, in the Yukon and Northwest Territories, tectonic influences also arise from the continuing compression and subduction processes along the northeastern edge of the Pacific plate. This area has seen significant crustal shortening and thickening, forming major thrust fault systems that uplift the interior and the Coast Mountains and play a central role in the region's structural complexities.

The ongoing collision of oceanic and continental plates, combined with ancient cratonic foundations, creates significant lithospheric heterogeneities and diverse geological structures. These variations influence how tectonic forces are distributed across the region, affecting stress accumulation, seismic activity, and crustal deformation. As a result, Western Canada serves as a prime location for studying both active tectonic processes and the long-term evolution of a transpressional continental margin system.

1.2 Ambient Noise Tomography

Seismic tomography uses the travel time, phase, or other properties of seismic waves to infer the velocity structure of the Earth. Among different tomographic methods, this study employs ambient noise tomography (ANT) to investigate seismic velocity variations beneath western Canada. ANT has recently become a well-established velocity mapping technique (e.g., Fulton, 1989; Sabra et al., 2005; Shapiro et al., 2005; Bensen et al., 2009; Behr et al., 2011; Ritzwoller et al., 2011). ANT utilizes ambient seismic noise to image the Earth's subsurface. This noise originates from both natural (e.g., ocean waves, atmospheric pressure variations, and earthquakes) and anthropogenic sources (e.g., traffic, industrial activities) (Behr et al., 2011). ANT is a passive technique that requires continuous monitoring of the subsurface without the need for active seismic sources, making it ideal for long-term seismic observation programs. This non-invasive approach makes ANT environmentally friendly and ideal for sensitive areas where active methods are impractical or undesirable.

One of the key strengths of ANT is its ability to produce high-resolution images of the Earth's crust and uppermost mantle with many crossing ray paths. The work of Sabra et al. (2005) in southern California demonstrated the potential of ANT to provide high-resolution seismic velocity models in tectonically active regions. Conversely, in tectonically quiet regions or areas where earthquakes are rare, ANT provides a reliable method for studying the subsurface. Continuous data acquisition in ANT enables tracking of changes in seismic velocity that may signal the movement of magma in volcanic regions, strain accumulation along faults, or other dynamic processes in the Earth's crust. The rapid expansion of global, regional, and local broadband seismograph networks has promoted its recent widespread adoption. Efficient seismic data management and distribution, as well as increasing computational capacity, have only recently made processing the large volumes of ambient seismic noise data involved possible.

Ambient noise spans a range of frequencies, typically from 0.001 Hz to 50 Hz. Different sources contribute to various parts of this frequency spectrum (Bensen et al., 2007):

1. Low-frequency noise (0.01 - 0.1 Hz) is mainly due to ocean waves and is sporadically excited by seismic waves from large earthquakes.

2. Intermediate frequencies (0.1 - 1 Hz) often result from high-frequency ocean waves, atmospheric disturbances, and seismic activity.

3. High-frequency noise (1 Hz and above) is dominated by anthropogenic sources like traffic, industrial activities, and local environmental factors (e.g., wind interacting with buildings, natural vegetation, or terrain).

Ambient noise is often non-directional, or diffusive, meaning the energy propagates in all directions. This contrasts with seismic waves from earthquakes, which travel in specific ray path directions from the hypocenter. In coastal regions, ambient noise may have a dominant direction related to asymmetrical ocean wave activity since microseisms generated by ocean waves propagate from the ocean floor toward land. This directional variability is important to consider because uneven noise-source distribution can influence the strength and reliability of interstation cross-correlations used in ambient noise tomography.

The data used in this study were selected from the EarthScope Data Management Center (DMC). The study focuses on Rayleigh wave phase velocities from 6.0 to 60.0 s period, which are sensitive to crustal and uppermost-mantle structure. Shorter periods are more sensitive to shallow crustal structure, while longer periods sample deeper parts of the lithosphere. In addition to phase velocity maps, this study uses shear wave velocity (Vs) depth slices to better interpret the crustal and uppermost-mantle structure beneath western Canada. Because phase velocity at each period is sensitive to a range of depths, Vs inversion provides a clearer depth-dependent view of the subsurface. In this thesis, Vs depth slices at 10, 20, 30, 40, and 50 km are used to examine the contrast between the low-velocity Cordillera and the high-velocity Canadian Shield.

Bensen et al. (2007) provided a detailed overview of the preprocessing techniques required for ambient noise data. Their study emphasized the importance of filtering and data normalization to extract reliable seismic velocity measurements from cross-correlation functions [Figure 5.2]. These preprocessing steps are directly relevant to this thesis as filtering isolates the frequency bands of interest, enhancing the signal-to-noise ratio. At the same time, data normalization reduces the influence of irregular noise sources, preventing artifacts in cross-correlation results. By following these techniques, this study improves the reliability of phase velocity measurements, leading to more accurate seismic imaging of the study region.

Ambient noise tomography based on cross-correlations of long recordings of seismic noise data has proven to be a powerful method for constructing surface wave velocity maps at short and intermediate periods. These surface wave maps provide constraints on crustal structure, which were difficult to obtain from traditional earthquake surface wave tomography due to studies the strong attenuation and scattering at short periods. A fundamental aspect of ANT is the cross-correlation of ambient seismic noise recorded at two distinct stations. This process can be mathematically represented as:

$$C_{ij}(\tau)=\int_{\infty}^{-\infty} u_i(t) \cdot u_j(t+\tau)dt$$

where $u_i(t)$ and $u_j(t)$ denote the ambient noise recordings at stations i and j, respectively, and τ represents the time lag. The resulting cross-correlation function, $C_{ij}(\tau)$, approximates the time derivative of Green's function between the two stations, effectively simulating the seismic response as if one station were a virtual source and the other a receiver. This approximation provides valuable insights into the Earth's velocity structure along the path connecting the stations. Therefore, the first set of phase measurements and phase speed inversions are performed across different period bands by filtering the broadband cross-correlations. This study focuses on 6.0 to 60.0 s periods as they provide optimal resolution for imagining the crust and uppermost mantle structures. Figure 5.2 presents the cross-correlation function, which is used as the base for the tomographic inversion process.

The surface waves extracted through this cross-correlation are dispersive, meaning that different frequencies propagate at varying velocities. Lower-frequency waves penetrate deeper into the Earth's interior, while higher-frequency waves are sensitive to shallower layers. By analyzing these frequency-dependent velocities, geoscientists can construct dispersion curves that depict how seismic velocity varies with depth, thereby facilitating the interpretation of the Earth's subsurface structure. In general, it can be described that the tomographic method generally involves four key steps:

1) creating reference 1-D models,

2) measuring phase velocities for each path,

3) performing 2-D phase velocity inversions,

4) developing a 3-D S-wave tomographic model by conducting a series of local 1-D inversions of phase velocities for surface velocity at all grid points.

In this study, ambient noise tomography is used to generate Rayleigh wave phase velocity maps across western Canada. These maps are then evaluated using uncertainty estimates, velocity perturbation patterns, and inversion convergence results. The phase velocity results are also used to develop shear wave velocity depth slices from 10 to 50 km depth. Together, these results help image the lithospheric contrast in Western Canada. While other geophysical datasets, such as gravity, magnetics, electrical conductivity, and heat-flow observations, can be integrated with seismic tomography to improve subsurface interpretation, this study focuses primarily on ambient-noise-derived seismic velocity structure.

Chapter 2

Tectonic Settings and Methodology

2.1 Introduction

Western Canada exhibits significant tectonic diversity and encompasses some of the most and least seismically active areas in Canada (Ristau et al., 2007). Western Canada contains the Rocky Mountains extending from British Columbia through Alberta and into the southern Yukon Territory. The main influences on the current tectonics of western Canada are the relative motion of the Pacific and North American plates along the west coast of North America and the subduction of the Juan de Fuca plate beneath North America (Ristau et al., 2007). Western Canada is defined as the region seaward of the Foreland Fold [Figure 5.3] and Thrust Belt, extending from the Canada-United States border in the south to areas where the subduction of the Pacific Plate and the Yakutat microplate beneath the North America Plate deforms the southern Alaskan lithosphere and uplifts mountain ranges (e.g., Finzel et al., 2015; Ristau, J. et al.,2007) [Figure 5.3].

2.2 Tectonic and Geologic Settings of Western Canada

Continents, in contrast to ocean basins, have a long and intricate tectonic history, evident in the seismic velocity variations in their crust and underlying mantle. The tectonic history of western Canada varies dramatically from west to east, and significant variations in lithospheric structure are associated with it, which will be explored in this study. The continental lithosphere of Canada offers a comprehensive record of tectonic events spanning the past 4 billion years, ranging from the ancient orogenic processes that formed the cratonic core to the ongoing deformation of the younger accreted terranes within the Canadian Cordillera. (Kao et al., 2013). This research addresses the geometry and behavior of the mantle lithosphere beneath western Canada, focusing on the current mantle structure, the thin lithosphere's origin in the southern Canadian Cordillera, and surface features linked to lithosphere delamination. Western Canada can be geologically divided into two primary regions: the elevated Canadian Cordillera to the west and the lower-lying North American craton to the east [Figure 5.3].

The Canadian Cordillera has high elevation, thin crust, and thin lithosphere compared to the adjacent craton. The Cordilleran Deformation Front marks the Cordillera's eastern topographic boundary, and the Rocky Mountain Trench (RMT) and Tintina Fault are interpreted to delineate the geological boundary between the craton and Cordillera (e.g., Hyndman & Lewis, 1999). The RMT is a structural basin formed through faulting, glacial erosion, and subsidence and serves as a significant geological boundary, separating the Rocky Mountains to the east from the Columbia and Cassiar Mountains to the west. The Tintina Fault is a major right-lateral (dextral) strike-slip fault that extends from northern British Columbia through the Yukon and into Alaska.

The craton forms the ancient core of North America and includes Archean and Proterozoic continental blocks (Dalton et al., 2011). These blocks form part of the crystalline crust and are underlain by cold, strong, and relatively thick mantle lithosphere. The cratonic region has lower elevation than the Cordillera and crustal thickness of approximately 40 km, while its lithosphere is much thicker than that of the Cordillera (Hyndman, 2017; Hasterok and Chapman, 2007; Chulick and Mooney, 2002). This difference in lithospheric thickness and thermal structure is important for this study because it is expected to make noticeable seismic velocity contrasts between the active Cordillera and the stable craton.

The western craton margin's tectonic history dates back approximately 750 million years, when the Rodinia supercontinent rifted, creating an ocean basin west of the continent (Burchfiel & Davis, 1975). Moreover, it established a continent-ocean boundary like the current one in eastern North America and the Atlantic Ocean basin. The tectonic setting shifted to plate convergence around 390 million years ago, resulting in subduction zones and a magmatic arc during the late Paleozoic and early Mesozoic (355-185 million years ago) (Monger & Price, 2002) [Figure 5.1]. Today, the cratonic crust is covered by the western Canadian Sedimentary Basin, an essential area for oil and gas resources. The Cordillera began forming 185 million years ago as plate convergence facilitated the addition of exotic terranes to the craton's western margin (e.g., Monger & Price, 2002), causing the North American plate to expand westward. The Canadian Cordillera's geological structure resulted from an extensive history of plate convergence and lateral material translation along strike-slip faults. The craton and Cordillera belong to the North American plate, with its western margin lying just offshore.

The western margin of the North American plate currently interacts with many major and minor oceanic plates with a complex system of convergent, transform, and transitional plate boundaries (Fluck et al.,2003) [Figure 5.1]. In the south, the Juan the Fuca Plate subducts beneath the North American Plate along the Cascadia subduction zone at an average convergence rate of ~40 mm/yr (DeMets and Dixon, 1999). To the north, the Queen Charlotte-Fairweather strike-slip fault system separates the North American and Pacific Plates and has a 55 mm/yr estimated relative dextral motion (DeMets and Dixon, 1999). A complex transitional tectonic regime separates the Cascadia subduction zone from the Queen Charlotte-Fairweather fault system. North of the Queen Charlotte fault, the Yakutat Terrane, which is moving northward on the Pacific Plate, is currently colliding with and being accreted to the North American Plate (Plafker et al., 1994). The Yakutat Terrane is an allochthonous terrane comprising of both oceanic and continental igneous and Cenozoic and Mesozoic sedimentary rocks (Plafker et al.,1994). The ongoing collision results directly in crustal deformation and uplift of the St. Elias Mountains and generates the high seismicity observed in the region. The collision is also believed to be the source of seismicity observed farther inland in the Mackenzie and Richardson Mountain ranges of the eastern Cordillera (Adams and Clague, 1993; Cassidy et al., 2001; Mazzotti and Hyndman, 2002). Northwest of the Yakutat collision zone, the Pacific Plate subducts beneath Alaska along the Aleutian subduction zone at ~55 mm/yr (DeMets and Dixon, 1999).

The current plate boundary geometry reflects the complex evolution of the Cordillera since the Eocene, shaped by the combination of subduction, collision, displacements along continental strike-slip faults, and accretion of terranes. The Cordillera is divided into distinct morphologic belts [Figure 5.3]: Insular Belt, Coast Belt, Intermontane Belt, Omineca Belt, and Foreland Belt (e.g., Gabrielse and Yorath, 1992). These belts contain numerous accreted terranes that are separated by major faults, suture zones, intrusive bodies, and metamorphic belts. The Cordillera is also characterized by extensive magmatism, including the Cascade volcanic arc in southwest Canada and magmatism within the Cordillera's interior. The most recent thermal-orogenic events are Cenozoic in the Cordillera, Proterozoic in the northern cratonic foreland where older basement is largely obscured, and Archean in the exposed craton.

Many hypotheses have been made about the tectonics of cordillera and craton. The accepted hypothesis proposes that Cordilleran terranes were added to the craton's western side via a series of east-dipping subduction zones (i.e., the same orientation as the present-day Cascadia subduction zone) [Figure 5.1]. Accretion mechanics remain debated, with one model suggesting that Cordilleran upper crust material placement above craton deep crust and mantle lithosphere (e.g., Cook et al., 2004) and another model suggesting that the entire Cordilleran lithosphere is exotic (e.g., Johnston, 2008). Alternatively, it has been proposed that plate convergence and accretion include periods of west-dipping subduction, whereby an oceanic plate outboard of the craton subducted below the Cordilleran terranes, and the final subduction of this oceanic plate resulted in a collision between craton and cordillera. Johnston (2008) suggested that this may have involved multiple subduction and collision events. In addition, it appears that the plate convergence was oblique, resulting in significant northward motion of the cordilleran blocks, as shown by palaeomagnetic studies of sedimentary and volcanic rocks (e.g., Enkin et al.,2006; Irving et al., 1995).

Hyndman et al. (2005) proposed that high temperatures beneath the Cordillera may be maintained by active small-scale convection. They suggested that long-term plate convergence and hydration from adjacent subduction systems may have reduced mantle viscosity and promoted vigorous convection. This process helps explain the warm and thin lithosphere beneath the Cordillera. In contrast, the cratonic lithosphere is older, colder, stronger, and more stable, which allows it to remain thicker over geological time. Therefore, the contrast between the Cordillera and the craton reflects differences in tectonic history, thermal structure, lithospheric strength, and mantle dynamics (e.g., Hyndman & Currie, 2011).

Moreover, the distribution of seismicity in the study region is the most important indicator of ongoing tectonic deformation. Fluck et al. (2003) described that seismicity is highest along the present-day plate boundaries (Cascadia subduction zone, Queen Charlotte strike-slip fault system, Yakutat collision zone). A large north-south variation in inland seismicity is observed in western Canada. The southern part has some low-level crustal seismicity, and the central part has very little seismicity. However, the northern part is characterized by quite high intraplate seismicity, especially along the Richardson Mountains shear zone and the Foreland Belt thrust zone [e.g., McKenzie Mountains (Cassidy et al., 2001)]. Thus, the Northern Cordillera is tectonically active today.

2.3 Previous Studies

The difference between the cordillera and craton is found in several different geophysical observations, including surface heat flow, crustal thickness, seismic tomography, and magnetotelluric observations. Geophysical observations from western Canada show a hot and thin lithosphere for the Cordillera compared to the adjacent cool, thick craton (Hyndman and Lewis, 1999). The change from the Phanerozoic mantle to the cratonic lithosphere is shown in tomographic models by a sharp increase in seismic velocities (Mercier et al., 2009).

Numerous studies have addressed the seismic and thermal structures of various parts of the Canadian Shield and Cordillera. Studies of western Canada's upper-mantle velocity structure began more than three decades ago when Buchbinder and Poupinet (1977), Wickens (1977), and Wickens and Buchbinder (1980) used short-period P-waves, surface-wave, and long-period S-wave travel time residuals, respectively, to document a low-velocity region beneath British Columbia. After that, global and continental-scale studies that include western Canada using both body waves (e.g., Grand et al., 1997; Frederiksen et al., 1998) and surface waves (e.g., Fouch et al., 2004; Tilmann, 2001) have imaged a relatively sharp mantle transition from low velocity in the east to high velocity in the west across the Cordilleran deformation front.

A few continental-scale seismic velocity models were obtained from surface-wave based measurements and waveform fitting approaches (e.g., Frederiksen et al., 2001; Bedle & Van der Lee, 2009; Yuan et al., 2011; Schaeffer & Lebedev, 2014). These provide evidence that the cordilleran lithosphere has lower seismic velocities compared to those of the adjacent Canadian Shield, which is interpreted as increased upper mantle temperatures beneath the Cordillera. However, they did not discuss the high velocities in the craton region. In western Canada, Kao et al. (2013) utilized ambient noise tomography, which provides better resolution of crustal structures than earlier tomographic models, as well as the sedimentary basins in western Canada and the Cordillera. [Figure 5.4]. Further, Hyndman & Currie (2011) argued that the high Cordilleran elevations result from the hot, low-density Cordilleran mantle. The thermal boundary between the cordillera and craton approximately coincides with the RMT-Tintina Fault system at the Earth's surface (Hyndman & Lewis, 1999). Mercier et al. (2009) represented the results of upper mantle teleseismic body-wave tomography throughout western Canada. In these models, high velocities are observed within the eastern part of the study area, whereas low velocities are observed within the western part. In the southern Cordillera, the transition from low seismic velocities in the west to higher velocities in the east is well defined at depths of 100-200 km and approximately follows the Cordilleran Deformation Front. However, this transition is less clearly resolved in the northern Cordillera. Also, Chen et al. (2019) conducted a tomographic analysis, revealing that the topography of the transition from thin to thick lithosphere is a significant feature for understanding the tectonic assembly of western Canada. However, their model only resolved structures at scales of approximately 200 km, which limits the ability to image finer variations across the Cordillera-craton boundary. All the studies used various tomography methods such as teleseismic, body wave velocity, group velocity, ambient noise tomography, etc., and described the different portions of the lithosphere in western Canada differently. However, these existing studies are either global/continental-scale, limited to low resolution, or local and lack a broader perspective. Meanwhile, this thesis uses improved station coverage and ambient noise tomography to generate higher-resolution phase velocity and Vs images, allowing a more detailed characterization of how this lithospheric transition is expressed within the crust and upper mantle.

This study aims to broaden the previous ANT research by shifting the focus to the southern part of western Canada, adding new data, and providing high-resolution phase velocity maps. Earlier work, such as that by Kao et al. (2013), provided a comprehensive analysis of crust and upper mantle shear velocity structures across Canada using ANT using fewer seismographs in western Canada than we do. Their research highlighted the contrast between the cold, stable Canadian Shield and the hot, tectonically active Cordillera. They suggest that the low density and low rigidity associated with an observed low V_S anomaly play a primary role in localizing the ongoing uplift and thrust-dominated seismicity of the Mackenzie Mountains. The current study area centers on the southwestern portion of western Canada (48-62°N and 112-141°W), where improved station coverage is available. The deployment of stations from several portable experiments i.e., the Canadian National Seismic Network (CNSN), the Canadian Northwest Experiment (CANOE), the Portable Observatories for Lithospheric Analysis and Research Investigating Seismicity (POLARIS) has filled some significant gaps in station coverage [Figure

5.5a] and allowed a broader scale study (e.g., Eaton et al., 2007; Clowes et al., 1999). This thesis exploits newly available and previously analyzed broadband data to examine the large-scale lithospheric surface wave velocity structure beneath western Canada [Figure 5.5a]. The enhanced spatial distribution of seismic stations in this area shows a high-resolution phase velocity and Vs maps from previous studies. Moreover, the northeastern region contains key geological features such as the RMT and Tintina Fault, which represent significant lithospheric transitions. A detailed understanding of how the transition in seismic velocity from craton to Cordillera is accommodated requires a consistent and systematic approach spanning the entire region. Also, this transition is vital for interpreting the geometry of the lithosphere and its interactions with the deeper mantle. For this reason, we focus our attention on the location of the Cordillera-craton transition. This study uses ANT techniques to resolve lateral velocity variations, particularly within the uppermost 80 km of the lithosphere. This comprehensively captures the transitions between the cold, thick, cratonic lithosphere and the hot, thin Cordilleran lithosphere and interprets the region's lithospheric structure and dynamics more precisely.

2.4 Research Objectives

The main research objective of this project is to interpret the geometry of the lithosphere from a broad, regional point of view in western Canada and focus on the geometry of the transition from west to east as discussed by Chen et al. (2019) where they identified low velocity anomalies beneath the southern Canadian Cordillera and high velocities on the eastern side, specifically under the Alberta foreland basin. Resolved velocities extend to a depth of 80 km. Using shear wave velocity inferred from ambient noise tomography to image western Canada reveals lateral velocity variations in the upper 80 km of the lithosphere and produces higher resolution images of this part of the crust and upper mantle. This thesis work contributes our understanding of western Canada.

2.5 Data and Method

We downloaded 6,662 day-long vertical-component seismic waveform data from over 100 broadband seismic stations spread across western Canada, providing comprehensive coverage of the region [Figure 5.5a]. This waveform data, obtained from the EarthScope Data Management Center through two channels called:

1. LHZ (Long-period high-gain vertical channel). It is designed to capture long-period (low-frequency) seismic waves, typically in the range of 0.01 to 0.1 Hz.

2. BHZ (Broadband high-gain vertical channel). It measures a broader frequency range, often from 0.1 to 50 Hz, capturing both long-period and short-period seismic waves.

Data was downloaded through the EarthScope Data Management Center, and Natural Resources Canada. These include: the) CAnadian Northwest Experiment [CANOE] (e.g., Mercier et al., 2009), the Canadian Rockies and Alberta Network (e.g., Rondenay et al., 2000), the Canadian National Seismograph Network [CNSN] (Kao et al., 2013), and Portable Observatories for Lithospheric Analysis and Research Investigating Seismicity [POLARIS] (e.g., Eaton et al., 2005) networks between 2003 and 2009 (e.g., Clowes et al., 1999). We use broadband seismographs from stations in the region of 48-62°N and 112-141°W that were emplaced between January 2000 to June 2024 [Figure 5.5a and 5.5b].

The data processing approach is based on the method proposed by Bensen et al. (2008). Initially, day-long vertical-component seismograms are downloaded from all accessible stations [Figure 5.5a and 5.5b]. Data conditioning involves removing the mean (average of amplitude values of the recorded signal over time) and trend from the data. It is used to remove bias (offset) in seismic signals. Then, tapering and eliminating the instrument response are applied to ensure that the transition at the start and end of a time window does not introduce artificial high-frequency noise and remove sensor-specific distortions. After that, spectral whitening is applied to enhance the signal quality. Spectral whitening is a signal processing technique that balances the amplitude of different frequency components in seismic data.

The daily cross-correlations were computed between vertical-component records for all available station pairs to extract Rayleigh wave signals. These daily cross-correlations were then stacked into monthly records, and the monthly stacks were further combined to produce yearly cross-correlation functions used for phase velocity measurements. In constructing the yearly stack, the monthly stacks are weighed by the number of days from which the monthly stack was made. This is done so that months for which relatively few days were available are given less weight

(Dalton et al., 2011). During the correlation process, some incomplete or invalid data are stored that are removed to maintain the quality and reliability of the dataset. It is necessary to clean and average the data to derive phase velocity measurements from the symmetric correlation data.

After data processing, the cleaned and stacked cross-correlation functions are used to measure Rayleigh wave phase velocities at selected periods. These phase velocity measurements are then used in the tomographic inversion to generate two-dimensional phase velocity maps [Figure 5.6a & 5.6b]. In this study, the inversion is performed for periods from 6.0 to 60.0 s. The inversion also provides uncertainty [Figure 5.7a & 5.7b] estimates, which are used to evaluate which parts of the model are better constrained and which areas should be interpreted more cautiously. Inversion convergence was also evaluated using convergence plots for each period [Figure 5.8], providing an additional check on the reliability of the phase velocity models. After that, Velocity perturbation maps [Figure 5.9] were calculated from the phase velocity results. These maps show the percentage of deviation of phase velocity from the regional average at each period. This step was used to represent relative velocity variations in a normalized form before developing the depth-dependent velocity model.

Shear wave velocity (Vs) is then used to provide a more depth-specific interpretation of the subsurface structure. Phase velocity maps show lateral velocity variations at different periods, but each period is sensitive to a broad range of depths rather than one exact depth level. Therefore, phase velocity maps are useful for identifying general velocity patterns, while Vs depth slices help separate shallow crustal structure from deeper lithospheric structure. In this study, the period-dependent phase velocity results are used to develop Vs depth slices at 10, 20, 30, 40, and 50 km [Figure 5.10]. These depth slices allow the Cordillera-craton contrast to be examined more clearly with depth.

Before inverting the phase velocity dispersion curves into shear wave velocity (Vs) depth profiles, it is important to understand the depth range sampled by Rayleigh waves at different periods. Rayleigh waves are dispersive, meaning that waves with different periods are sensitive to different depths. Shorter-period waves mainly sample the shallow crust, while longer-period waves are sensitive to deeper crustal and upper-mantle structure.

In this study, Rayleigh wave depth sensitivity kernels [Figure 5.11] were used to evaluate how phase velocity at each period responds to variations in shear wave velocity with depth. Figure

5.11 shows the sensitivity kernels for periods of 6.0, 7.5, 10.0, 20.0, 30.0, and 60.0 s. These kernels were computed using a reference one-dimensional crustal and upper-mantle velocity model representative of the average structure of western Canada.

The sensitivity kernels [Figure 5.11] show that the 6.0 and 7.5 s periods are mainly sensitive to the shallow upper crust, approximately between 5 and 12 km depth. The 10.0 s period is sensitive to the upper to middle crust, approximately between 8 and 15 km depth. The 20.0 s period samples the middle to lower crust, roughly between 15 and 35 km depth. The 30.0 s period reaches the lower crust and uppermost mantle, approximately between 25 and 50 km depth. The 60.0 s period samples deeper upper-mantle structure, with sensitivity extending to approximately 50-100 km depth. These kernels confirm that Rayleigh waves sample progressively greater depths as period increases.

The sensitivity kernels [Figure 5.11] provide the depth basis for converting period-dependent phase velocity dispersion curves into Vs structure. Phase velocity maps show lateral velocity variations at different periods, but each period is sensitive to a range of depths rather than a single depth level. Therefore, the phase velocity results were further inverted to obtain Vs depth slices at 10, 20, 30, 40, and 50 km. These depth slices allow the crustal and uppermost-mantle structure to be interpreted more directly and help distinguish shallow crustal heterogeneity from deeper lithospheric variations.

In addition to shear wave velocity sensitivity, Rayleigh wave phase velocity can also have secondary sensitivity to compressional wave velocity (Vp) and density. However, the sensitivity to Vs is usually strongest, while the sensitivity to Vp is smaller and the sensitivity to density is weaker and more depth dependent. For this reason, Vs is treated as the primary parameter in depth inversion, while Vp and density are constrained using the reference model or empirical scaling relations. This approach allows the final Vs model to focus on the main structural variations needed to interpret the Cordillera-craton transition beneath western Canada.

The final outputs of the workflow include phase velocity maps [Figure 5.6a & 5.6b], uncertainty maps [Figure 5.7a & 5.7b], inversion convergence plot [Figure 5.8] velocity perturbation maps [Figure 5.9], and Vs depth slices [Figure 5.10] results. Together, these results provide the basis for interpreting the lithospheric structure beneath western Canada, especially the contrast between the low-velocity Cordillera and the high-velocity Canadian Shield.

Chapter 3

Results and Discussion

3.1 Results

3.1.1 Phase Velocity and Uncertainty Maps

Phase velocity refers to the speed at which a particular phase of a surface wave propagates through the Earth. It is frequency-dependent, with lower frequencies being sensitive to velocity variations in deeper parts of the earth. It provides essential information about the properties and structure of the Earth's crust and mantle, such as variations in rock rigidity, density, thickness and layering, as well as temperature, upwelling, deformation and composition. (e.g., Shapiro et al., 2005; Bensen et al., 2007; Lin et al., 2008). In ambient noise tomography (ANT), Rayleigh wave phase velocities are extracted from cross-correlated seismic noise and are especially useful for imaging Earth's crustal structure and lithospheric characteristics (Bensen et al., 2007).

A phase velocity map [Figure 5.6a & 5.6b] represents the spatial distribution of these velocities at a given period across a study area. In this study, these phase velocity maps are the primary input for depth inversion to obtain shear wave velocity as a function of depth. Since each period is sensitive to a range of depths defined by the Rayleigh wave depth sensitivity kernel, these maps provide indirect information about crustal and lithospheric structure rather than a direct depth slice.

Uncertainty maps [Figure 5.7a & 5.7b] show how reliable the velocity results are in different parts of the study area. In this study, phase velocity estimates with uncertainty values below ~0.05 km/s are considered well constrained and suitable for interpretation. Values between ~0.05 and 0.08 km/s are useful for identifying broad regional patterns. Areas with uncertainty greater than ~0.08-0.10 km/s are less reliable, especially near the model edges and at longer periods. Therefore, the interpretation mainly focuses on phase velocity patterns that occur in areas with uncertainty below ~0.05 km/s.

6.0 s Period: The 6.0 s phase velocity [Figure 5.6a] result reflects shallow crustal structure in western Canada. The velocity ranges from about 2.8 to 3.4 km/s. Lower velocities are observed in the southern and south-central part of the study area, especially around southern British Columbia, and the Cordilleran region. Higher velocities appear along the coastal British Columbia and toward northern Alberta. Since 6.0 s Rayleigh waves are sensitive to shallow depths, these velocity variations are associated with upper-crustal heterogeneity rather than deeper lithospheric structure. The uncertainty result [Figure 5.7a] shows lower standard deviation across the interior British Columbia-Alberta region, while higher uncertainty is observed toward the offshore Pacific side, the Yukon side, and the far eastern part of the study area. This indicates that the velocity pattern is more stable in the better-constrained onshore region and less stable in areas with weaker data constraints.

6.67 s Period: The 6.67 s phase velocity map [Figure 5.6a] shows shallow crustal structure, with velocity ranging from about 2.8 to 3.4 km/s. The pattern looks similar to the 6.0 s map but slightly smoother, and the strong low-velocity zones in southern British Columbia become less prominent. Low velocities are still observed along the coastal British Columbia region and in parts of the central Cordillera, while higher velocities appear toward the northeastern interior near the Yukon and Alberta side. Because 6.67 s Rayleigh waves slightly deeper than 6.0 s, the shallow heterogeneity starts to smooth out at this period. The uncertainty map [Figure 5.7a] shows low standard deviation across the interior British Columbia-Alberta region, while higher uncertainty appears along the offshore Pacific, the Yukon side, and the far eastern part of the study area. It presents the velocity pattern is more reliable in the central onshore region.

7.5 s Period: The 7.5 s phase velocity map [Figure 5.6a] reflects upper-crustal structure, with velocity ranging from about 2.8 to 3.4 km/s. The velocity pattern becomes more uniform, and the strong low-velocity zones in southern British Columbia gradually fade. Low-velocity regions remain along the coastal British Columbia area and the central Cordillera, while higher velocities continue to appear toward the northeastern interior, where the stable craton begins to dominate. The contrast between the Cordillera and the craton becomes clearer at this period. The uncertainty map [Figure 5.7a] shows low standard deviation across the central onshore region, while higher uncertainty appears along the offshore Pacific, the northern Yukon side, and the far eastern part, showing that the model is well constrained in the interior.

10.0 s Period: The 10.0 s phase velocity map [Figure 5.6a] provides insights into the mid-crustal structure, with velocity ranging from about 2.8 to 3.6 km/s. The overall background velocity becomes higher, and the low-velocity anomalies along the Cordillera become more diffuse. Higher velocities appear more clearly toward the northeastern interior, while the Coast Mountains and southern British Columbia still show low velocities, suggesting thicker or warmer crust in the Cordilleran region. This period highlights the growing contrast between the active Cordillera and the stable craton. The uncertainty map [Figure 5.7a] shows low standard deviation across central study area, while higher uncertainty appears along the offshore Pacific, the northern Yukon margin, and the far eastern part.

12.0 s Period: The 12.0 s phase velocity map [Figure 5.6a] reflects mid-crustal structure, with velocity ranging from about 2.8 to 3.7 km/s. The velocity pattern becomes smoother, and the Cordillera-craton contrast becomes more visible. Low velocities are observed in the southern Cordillera and parts of coastal British Columbia, suggesting warmer or thicker crust, while the northeastern interior shows high velocities consistent with the stable craton. This period shows that mid-crustal heterogeneity is still influenced by tectonic activity along the Cordillera. The uncertainty map [Figure 5.7a] shows low standard deviation across the central interior, while higher uncertainty appears along the offshore Pacific, the Yukon side, and the southwestern coastal region.

15.0 s Period: The 15.0 s phase velocity map [Figure 5.6b] provides insights into a slightly deeper upper to middle crustal structure, with velocity ranging from about 3.2 to 3.8 km/s. The high-velocity regions associated with the stable craton continue to dominate the northeastern part, while the low-velocity zones now extend further inland from the coastal areas. This indicates that the effects of tectonic activities are not confined to the immediate coastal regions but also influence areas further east. This period highlights the potential interactions between deeper crustal processes, particularly near the subduction zones. The uncertainty map [Figure 5.7b] shows low standard deviation across the central onshore region, while higher uncertainty appears along the offshore Pacific, the northern Yukon, and the far eastern part.

20.0 s Period: The 20.0 s phase velocity map [Figure 5.6b] reflects the lower crust and the uppermost mantle, with velocity ranging from about 3.2 to 3.9 km/s. The Cordillera-craton contrast becomes much sharper, with clear low-velocity zones along the Coast Mountains and the southern

Cordillera, suggesting warmer or more deformed lithosphere. Higher velocities dominate the northeastern part, consistent with the cold and stable cratonic lithosphere. This period shows the transition from active tectonic regions in the west to the stable craton in the east. The uncertainty map [Figure 5.7b] shows low standard deviation across the central study area, while higher uncertainty appears along the offshore Pacific, the northwestern Yukon, and the far eastern boundary.

30.0 s Period: The 30.0 s phase velocity map [Figure 5.6b] represents the uppermost-mantle structure, with velocity ranging from about 3.4 to 4.0 km/s. The Cordillera-craton contrast becomes stronger. Low velocities dominate the western Cordillera, especially along the Coast Mountains and southern British Columbia and high velocities mark the cratonic lithosphere in the northeastern part. A clear high-velocity zone is visible across the northern interior, which suggests the cold and thick craton. This period highlights the deeper lithospheric structure beneath western Canada. The uncertainty map [Figure 5.7b] shows low standard deviation across the interior of the study region, while higher uncertainty appears along the offshore Pacific, the northern Yukon side, and the far eastern part.

60.0 s Period: The 60.0 s phase velocity map [Figure 5.6b] reflects deeper upper-mantle structure, with velocity ranging from about 3.6 to 4.2 km/s. The Cordillera-craton contrast becomes the dominant feature, with low velocities under the western Cordillera and high velocities under the craton to the northeast. This period highlights the deeper mantle structure and the lithospheric difference between the active Cordillera and the stable craton. The uncertainty map [Figure 5.7b] shows low standard deviation across the central interior, and higher uncertainty appears along the offshore Pacific, the northern Yukon margin, and the far eastern part.

3.1.2 Velocity Perturbation Maps

The velocity perturbation maps [Figure 5.9] dc/c (%) show how the phase velocity at each period deviates from the regional average, where red colors represent negative perturbations, blue colors represent positive perturbations, and white colors represent values close to zero, with perturbations ranging from about -4% to +4%. The maps were also masked using the corresponding uncertainty maps, so poorly constrained areas that are excluded from interpretation. At the shorter periods (6.0-

7.5 s), negative perturbations of about -2% to -4% dominate the southern Cordillera and central British Columbia, while positive perturbations of about +2% to +4% appear along the northern edge and the northeastern Alberta region. At the intermediate periods (10.0-20.0 s), the perturbation pattern becomes more organized, with negative anomalies along the western Cordillera and positive anomalies toward the northeastern craton. At the longer periods (30.0 s and 60.0 s), the perturbation contrast becomes strongest, with widespread positive anomalies across the craton and negative anomalies along the western Cordillera, reflecting the sharp lithospheric contrast between the Cordilleran and cratonic mantle.

3.1.3 Shear wave velocity at various Depth

The Vs depth slices presented here are derived from the period-dependent Rayleigh wave phase velocity results using the depth sensitivity and inversion approach described in Chapter Two.

Vs at 10 km depth: The Vs map at 10 km depth [Figure 5.10] reflects the upper crustal shear wave velocity structure, with velocity ranging from about 3.2 to 3.7 km/s. Low velocities of about 3.2-3.4 km/s are observed across most of the central part of British Columbia and Alberta, reflecting the thick sedimentary cover of the Western Canada Sedimentary Basin and the felsic upper crustal composition. Higher velocities of about 3.5-3.7 km/s appear along the coastal British Columbia and the northeastern margin, where the crust is more consolidated. The overall pattern suggests that the 10 km depth slice reflects shallow crustal features rather than the deeper cratonic structure.

Vs at 20 km depth: The Vs map at 20 km depth [Figure 5.10] represents the middle crustal structure, with velocity ranging from about 3.2 to 4.2 km/s. The overall velocity becomes higher than at 10 km, and the Cordillera-craton contrast starts to appear more clearly. Low velocities of about 3.4-3.6 km/s remain visible along the western Cordillera and southern British Columbia, suggesting warmer or more deformed mid-crust. Higher velocities of about 3.8-4.0 km/s appear toward the northeastern interior, while several localized high velocity zones (around 4.0-4.2 km/s) are observed in central and southern British Columbia. These anomalies may indicate more rigid mid-crustal materials or localized variations in crustal composition and structure.

Vs at 30 km depth: The Vs map at 30 km depth [Figure 5.10] reflects the lower crust to uppermost mantle structure, with velocity ranging from about 3.4 to 4.6 km/s. The Cordillera-craton contrast becomes strong at this depth. Low velocities of about 3.4-3.8 km/s are observed in the western Cordillera, the Coast Mountains, and the northern margin near the Yukon, suggesting warmer or thinner crust in the active tectonic region. In contrast, high velocities of about 4.2-4.6 km/s appear across the central and eastern interior, presenting the transition from the lower crust into the cratonic uppermost mantle.

Vs at 40 km depth: The Vs map at 40 km depth [Figure 5.10] represents the uppermost mantle structure, with velocity ranging from about 3.6 to 4.6 km/s. The Cordillera-craton contrast remains clearly visible. Low velocities of about 3.6-4.0 km/s are observed along the Cordillera, the Coast Mountains, and parts of the western margin, suggesting a warmer or thinner mantle in the active region. High velocities of about 4.2-4.6 km/s dominate the central and eastern parts of the study area, with high velocity zones across the craton, consistent with the cold and thick mantle lithosphere of the Canadian Shield. This depth presents the clearest contrast between the Cordillera and the craton.

Vs at 50 km depth: The Vs map at 50 km depth [Figure 5.10] reflects the deeper upper mantle structure, with velocity ranging from about 3.8 to 4.6 km/s. The Cordillera-craton contrast continues to be clearly expressed. Low velocities of about 3.8-4.0 km/s remain visible along the western Cordillera and parts of the southern coastal margin, suggesting warm and thin mantle lithosphere beneath the active region. High velocities of about 4.4-4.6 km/s reflect the craton and the central part of the study area, which suggests cold and thick cratonic mantle. The strong velocity gradient between the Cordillera and the craton at this depth supports a sharp lithospheric transition in western Canada.

3.2 Discussion

Before interpreting the velocity patterns geologically, it is important to consider the spatial resolution of the tomographic model. The results provide high-resolution images across much of the study area, but resolution is lower in regions where ray paths are sparse or strongly aligned in one direction. Therefore, some elongated velocity features may reflect ray-path geometry rather than true subsurface structure. The discussion below focuses mainly on broad, repeatable patterns that are consistent across periods and supported by lower uncertainty.

3.2.1 Interpretation of Tectonic Features

The Vs depth slices [Figure 5.10] provide a clearer depth-dependent interpretation of the crustal and upper mantle structure beneath western Canada than the period-based phase velocity maps. While the phase velocity maps show lateral velocity variations at different periods, the Vs slices allow these variations to be examined at specific depths. This makes it easier to distinguish shallow crustal features from deeper lithospheric structures.

High-Velocity Regions: Higher Vs values are observed toward the central, northeastern, and eastern parts of the study area, where the cratonic interior becomes more expressed with depth. At 30 km depth and below, Vs values reach 4.2-4.6 km/s, and these high velocities persist at 40 and 50 km depths. This pattern indicates the presence of colder, stronger, and thicker lithospheric material associated with the Canadian Shield and its cratonic mantle root.

Low-Velocity Regions: The western Cordillera is characterized by lower Vs values, especially along coastal British Columbia, the Coast Mountains, and the tectonically active western margin. These lower velocities suggest a warmer, thinner, and more deformed lithosphere, which is consistent with the active tectonic setting of western Canada and the influence of the nearby Juan de Fuca subduction system.

Overall, the Vs depth slices show that the velocity structure beneath western Canada is controlled by a major lithospheric contrast between the tectonically active Cordillera in the west and the stable cratonic interior to the east and northeast. This contrast becomes more distinct with increasing depth, suggesting that the shallow crustal heterogeneity gradually gives way to a deeper lithospheric-scale boundary between these two tectonic domains. These depth-dependent patterns show that the Cordillera-craton transition extends beyond the shallow crust and continues into the upper mantle. In addition, these Vs depth slices provide a useful framework for future studies that aim to improve the interpretation of lithospheric structure beneath western Canada.

3.2.2 Effect of Velocity Variation in Western Canada

Crustal and Mantle Dynamics: The Vs depth slices [Figure 5.10] highlight a visible contrast between the stable cratonic lithosphere in the northeast and the more tectonically complex Cordillera to the west. High Vs in the craton at all depths is consistent with cold, thick, and uniform lithosphere, while lower Vs along the western margin reflects a more heterogeneous structure influenced by active tectonics.

Within the crust (10-30 km depth), the contrast between the two regions is already evident. At 10 km depth, the Cordillera shows Vs values of approximately 3.2-3.4 km/s compared to 3.4-3.6 km/s in the craton. This difference becomes more prominent at 20-30 km depth, where the Cordillera presents Vs of 3.2-3.8 km/s while the craton reaches 3.8-4.6 km/s, indicating a different crustal composition and thermal state between the two regions.

At lithospheric mantle depths (40-50 km), the contrast persists and remains strong. The Cordillera shows Vs values of approximately 3.6-4.2 km/s, while the craton maintains significantly higher values of 4.2-4.6 km/s. This sustained velocity difference indicates that the structural distinction between the two regions extends well into the lithospheric mantle [Figure 5.12], reflecting a fundamental difference in mantle composition [Figure 5.12], temperature, and tectonic history.

Assumption of Seismic Hazard: Although seismic hazard is controlled by many factors, Vs variations can help indicate where the lithosphere is weaker or more stable providing useful information for interpreting seismic hazards. The low Vs zones near the Cordillera, particularly at 10-30 km depth, suggest a more heterogeneous and thermally elevated crust compared to the craton. These regions broadly align with known active fault systems and complex crustal structures associated with the Cordilleran orogeny, which may indicate seismic hazards. In contrast, the high-Vs regions within the Canadian Shield reflect a colder and mechanically stable lithosphere. Although this study does not assess seismicity or hazard directly, the observed Vs patterns are consistent with existing geological interpretations that associate stable cratonic regions with lower tectonic activity and seismic hazards.

3.2.3 Geological Features and Velocity Variation

The Vs depth slices [Figure 5.10] reflect lateral variations across geological terranes [Figure 5.4] within the Cordillera, such as Wrangellia, Stikine, and Cache Creek. Terranes like Wrangellia and Stikine exhibit higher Vs values, particularly at 20-30 km depth, which may be attributed to their older, more consolidated crustal structures. In contrast, the Cache Creek terrane shows lower Vs values across all depth slices, which may result from a combination of crustal deformation, elevated temperatures, and heterogeneous lithology.

Across the region, Vs variations are influenced by crustal composition and thermal state [Figure 5.12]. Cordilleran terranes consist of felsic to intermediate igneous rocks, which are more silica-rich and therefore characterized by lower shear wave velocities. By contrast, the Canadian Shield comprises Archean and Paleoproterozoic gneisses and granitoid rocks that are compositionally felsic but reside within a cold and thick cratonic lithosphere. The high Vs in this region thus reflects stability rather than mafic composition. At greater depths (30-50 km) [Figure 5.10], temperature becomes main control on Vs, which explains the strong Cordillera-craton contrast at these depths.

Moreover, the low Vs values at 10 km depth [Figure 5.10] across the central interior of British Columbia and Alberta image the Western Canada Sedimentary Basin, reflecting unconsolidated, younger sediments and felsic crustal material. These low Vs anomalies become less prominent at 30-50 km depths, consistent with deeper, more competent geological structures. This depth-dependent variation highlights the strength of the Vs depth slices in distinguishing between surface sedimentary layers and underlying lithospheric structure [Figure 5.12], something that the phase velocity maps alone cannot resolve.

3.2.4 Volcanic Activity and Heat Flow

The Vs depth slices [Figure 5.10] provide additional insight into volcanic activity and associated heat flow in the study area. Regions with volcanic arcs, particularly along the Cache Creek terrane [Figure 5.4], show low Vs values in our results, especially at 10-20 km depths [Figure 5.10]. Cache Creek contains oceanic rocks, diverse lithologies, and tectonically deformed crust, suggesting a less consolidated and lower-rigidity lithosphere (Nelson et al., 2013). It is assumed that these low Vs values may be linked to higher temperatures underground, past volcanic activity, or geological complexity [Figure 5.12], which aligns with the terrane's accretion history. At greater depths (30-40 km) [Figure 5.10], persistent low Vs beneath the Cordillera may reflect zones of weaker lithospheric structure, potentially due to elevated heat flow and the presence of partial melt conditions in the uppermost mantle.

3.2.5 Inversion Convergence and Reliability

The convergence plots [Figure 5.8] of the Bayesian inversion show that the misfit values remain stable and well-bounded across all iterations for every period from 6.0 s to 60.0 s, confirming that the rjMcMC algorithm has properly converged at each period. This stable convergence supports the reliability of the phase velocity maps, which were then used to invert Vs depth slices [Figure 5.11]. The combination of well-converged Bayesian phase velocity maps and the subsequent Vs inversion at multiple depths provides a robust and reliable image of the lithospheric structure beneath western Canada.

3.3 Conclusion

This study applied ambient noise tomography with Bayesian trans-dimensional inversion to map the lithospheric geometry of western Canada using Rayleigh wave phase velocities at periods of 6.0 to 60.0s, derived from over one hundred broadband seismic stations. The resulting velocity then inverted to shear wave velocity (Vs) depth slices at 10, 20, 30, 40, and 50 km [Figure 5.10] provides a detailed and robust characterization of the crust and uppermost mantle across the study area.

The Vs depth slices [Figure 5.10] reveal a clear contrast between the active western Cordillera, characterized by low Vs values (3.2-4.0 km/s) reflecting warm, thin, and deformed lithosphere, and the stable Canadian Shield, characterized by high Vs values (4.2-4.6 km/s) reflecting cold, thick, and rigid cratonic lithosphere. At shallow depths (10 km), the Vs maps image the Western Canada Sedimentary Basin and the felsic upper crust. At intermediate depths (20-30 km), the Cordillera-craton contrast begins to emerge, with localized high-velocity zones representing deeper crustal blocks or mafic intrusions. At deeper levels (40-50 km), the Cordillera-craton contrast becomes the dominant feature, reflecting the fundamental lithospheric difference between the warm Cordillera and the cold craton.

The supporting phase velocity maps [Figure 5.6a & 5.6b], perturbation maps [Figure 5.8], and uncertainty estimates [Figure 5.7a & 5.7b], along with the stable convergence of the Bayesian inversion [Figure 5.8], confirm the reliability of the Vs results. Although direct evidence of current magmatic processes or thermal anomalies is not found in this study, persistent low Vs zones beneath the Cordillera may still reflect elevated heat flow, past volcanic activity, or compositional variations associated with the active subduction setting. Overall, the Vs depth slices [Figure 5.10] provide one of the most detailed images of the lithospheric structure beneath western Canada. It presents the shallow crustal heterogeneity and the deeper lithospheric segmentation between the tectonically active Cordillera and the stable craton.

Chapter 4

Future Work

4.1 Future Research Directions

This thesis successfully generated higher-resolution images of the lithospheric structure beneath western Canada using ambient noise tomography. This is the prime contribution of the study compared with many previous regional and continental-scale studies, which either covered broader areas at lower resolution or focused on selected parts of the Cordillera-craton system. The phase velocity maps, uncertainty estimates, velocity perturbation maps, and Vs depth slice maps produced in this thesis provide a more detailed view of the transition between the low-velocity Cordillera and the high-velocity craton. Therefore, future studies should not be viewed as completing the main objective of this work, but as extending, testing, and strengthening the resolved lithospheric model presented here. Although the present model provides a strong regional image of this transition, several future directions can improve the interpretation and broaden the scientific value of the work.

4.1.1 Refining and Validating the Resolved Lithospheric Model

The next step is to refine and validate the resolved velocity model developed in this thesis. The current phase velocity and Vs models already show the main lithospheric contrast across western Canada, but additional testing can help identify which smaller-scale velocity patterns are strongly resolved and which areas should be interpreted more cautiously.

Future studies could use additional resolution tests, such as checkerboard tests and synthetic recovery tests, to examine the stability of the observed velocity anomalies. These tests would help evaluate whether the low-velocity zones in the Cordillera and the high-velocity regions in the craton are consistently recovered under different model conditions. They would also be useful for examining areas where uncertainty is higher, especially near the offshore Pacific margin, the northern Yukon side, and the far eastern boundary of the model.

Different inversion parameters and starting models could also be tested to evaluate the sensitivity of the final Vs structure. Since Vs depth slices are derived from period-dependent phase velocity dispersion curves, testing the inversion setup would help confirm the robustness of the depth-dependent interpretation. This would strengthen the connection between the phase velocity maps and the final lithospheric interpretation.

4.1.2 Improving Data Coverage in Higher-Uncertainty Areas

Future research can build on this study by adding more seismic data from available stations. Improved station coverage would be especially useful in areas where the uncertainty maps show weaker constraints. Better data coverage can improve ray-path distribution, reduce edge effects, and help stabilize velocity estimates near the margins of the study area.

Additional vertical component data from suitable channels, such as HHZ where available, could also be included in future work after proper quality control and instrument-response correction. This would increase the number of usable records and may improve the reliability of phase velocity measurements. However, the purpose of adding such data would be not to replace the current model, but to further strengthen the resolved image produced in this thesis.

4.1.3 Improving the Inversion Framework

The inversion approach used in this thesis successfully generated phase velocity maps, uncertainty estimates, and Vs depth slices. However, future work can improve the technical framework of the inversion. It can also compare different inversion strategies to evaluate how model choices affect the final image. For example, future work could compare Bayesian inversion results with other regularized or trans-dimensional inversion approaches. Such comparison would help determine whether the main Cordillera-craton velocity contrast remains stable across different methods.

4.1.4 Integration with Other Geophysical Datasets

Although ambient noise tomography provides strong constraints on seismic velocity structure, future studies can improve interpretation by integrating the present results with other geophysical observations. Gravity, magnetotelluric, heat-flow, receiver function, and body-wave tomography datasets could all provide useful complementary information

Gravity data can help identify density variations related to crustal thickness, basin structure, and compositional changes. Magnetotelluric data can provide information about electrical conductivity, which may be influenced by fluids, melt, temperature, or hydrated minerals. Heat-flow observations can help test whether low-velocity regions are associated with elevated temperatures. Receiver functions can help constrain crustal thickness and major discontinuities, while body-wave tomography can extend the interpretation into deeper mantle structure.

Combining these datasets with the higher-resolution velocity model produced in this thesis would allow the Cordillera-craton transition to be interpreted more confidently. It would also help separate the effects of temperature, composition, lithospheric thickness, and deformation on the observed seismic velocity patterns.

4.1.5 Extending the Model to Greater Depths

The Vs depth slices in this thesis mainly image the crust and uppermost mantle, particularly from 10 to 50 km depth. Future research could extend the depth of investigation by using longer-period surface waves, teleseismic body waves, receiver functions, and geodynamic modeling. This would help examine whether the velocity contrast observed in the upper lithosphere continues into deeper mantle structure.

A deeper model would be useful for understanding how the Cordilleran lithosphere interacts with the underlying mantle. It could help test whether the thin lithosphere beneath the Cordillera is related to mantle upwelling, small-scale convection, subduction processes, or lithospheric removal. It could also clarify how the colder and thicker cratonic mantle changes toward the Cordilleran margin. Extending the model to greater depths would therefore help connect the crustal and uppermost-mantle structure imaged in this thesis with larger-scale mantle dynamics beneath western Canada.

4.1.7 Time-Lapse and Monitoring Applications

Although this thesis focuses on long-term lithospheric structure, future studies could apply ambient noise methods to time-lapse seismic monitoring in selected areas of western Canada. Time-lapse monitoring can detect small changes in seismic velocity over time, which may be related to stress changes, fluid movement, volcanic activity, or fault-zone processes.

This approach would be most useful in tectonically active regions such as the Cordillera, the Cascadia subduction zone, the Queen Charlotte Fault system, and other areas with active crustal deformation. However, this type of work would require stable station coverage, careful data quality control, and methods specifically designed to detect small temporal velocity changes. Time-lapse analysis would not replace the structural model developed in this thesis. Instead, it could build on the present results by examining whether parts of the active Cordillera show measurable temporal changes in seismic velocity.

4.1.7 Geological and Practical Applications

The resolved lithospheric model developed in this thesis can support broader geological interpretation of western Canada. A clearer image of the contrast between the Cordillera and the craton can help improve understanding of terrane boundaries, sedimentary basins, crustal thickness variation, fault systems, and lithospheric structure.

The results may also provide useful background information for future studies related to seismic hazard, geothermal systems, mineral exploration, and basin analysis. However, these applications would require additional targeted datasets and specific methods. The present thesis does not directly assess earthquake hazard or resource potential. Instead, it provides a structural framework that future studies can use as a foundation.

4.2 Summary

This thesis presents higher-resolution seismic images of the lithosphere beneath western Canada through phase velocity maps and Vs depth slices. Future studies can build on this work by testing the stability of the model, improving data coverage in higher-uncertainty areas, refining the inversion framework, and integrating other geophysical datasets. These steps would strengthen the interpretation of the Cordillera-craton transition and support future studies of lithospheric structure in western Canada.

Chapter 5

Figures

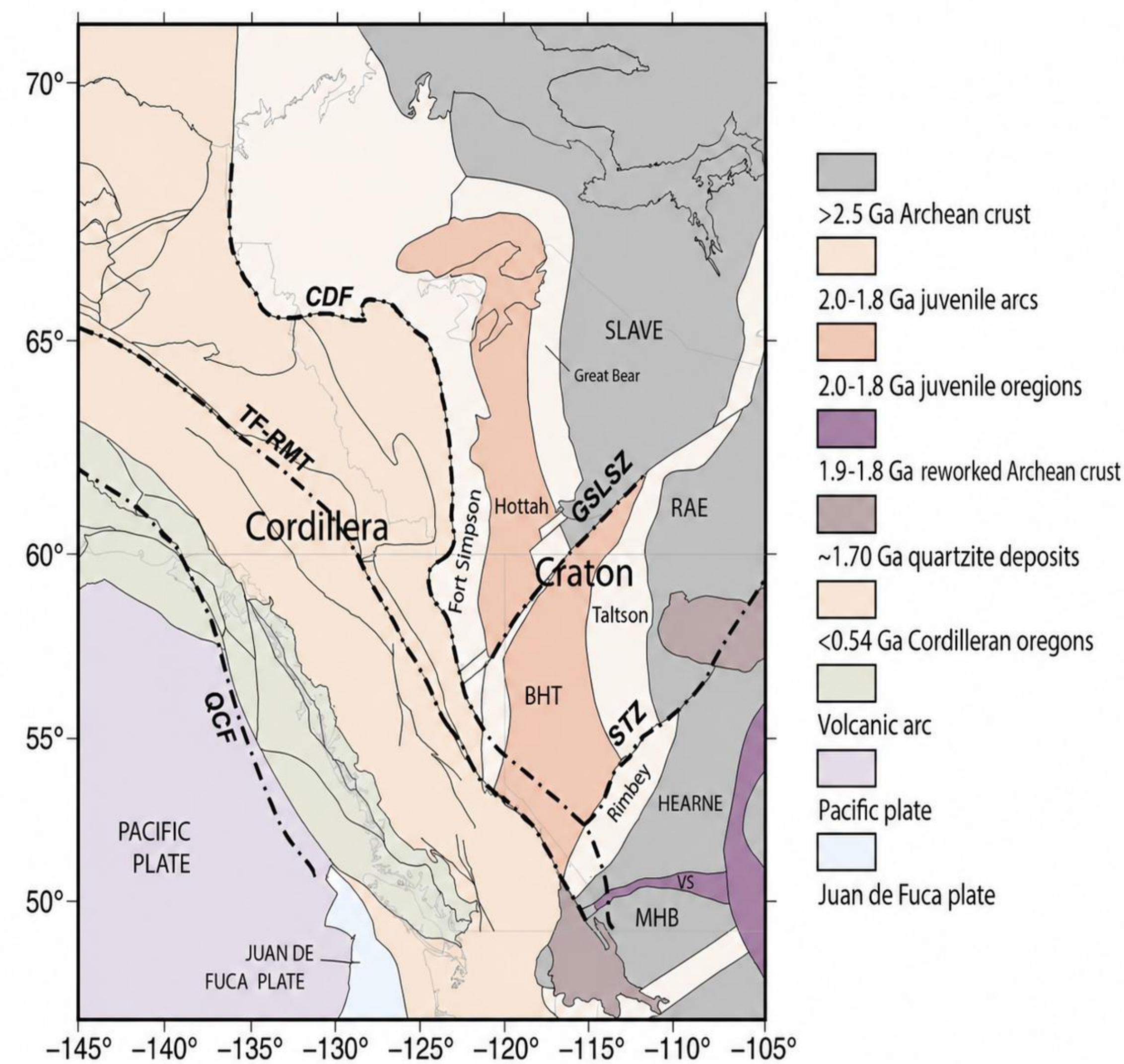

Figure 5.1: Tectonic map of western Canada (Whitmeyer & Karlstrom, 2007) shows the Cordillera orogenic belt and several Precambrian domains in the east. MHB: Medicine Hat Block, BHT: Buffalo Head Terrane, CDF: Cordilleran Deformation Front, QCF: Queen Charlotte Fault, TF-RMT: Tintina Fault-Rocky Mountain Trench, STZ: Snowbird Tectonic Zone, GSLSZ: Great Slave Lake Shear Zone, VS: Vulcan Structure.

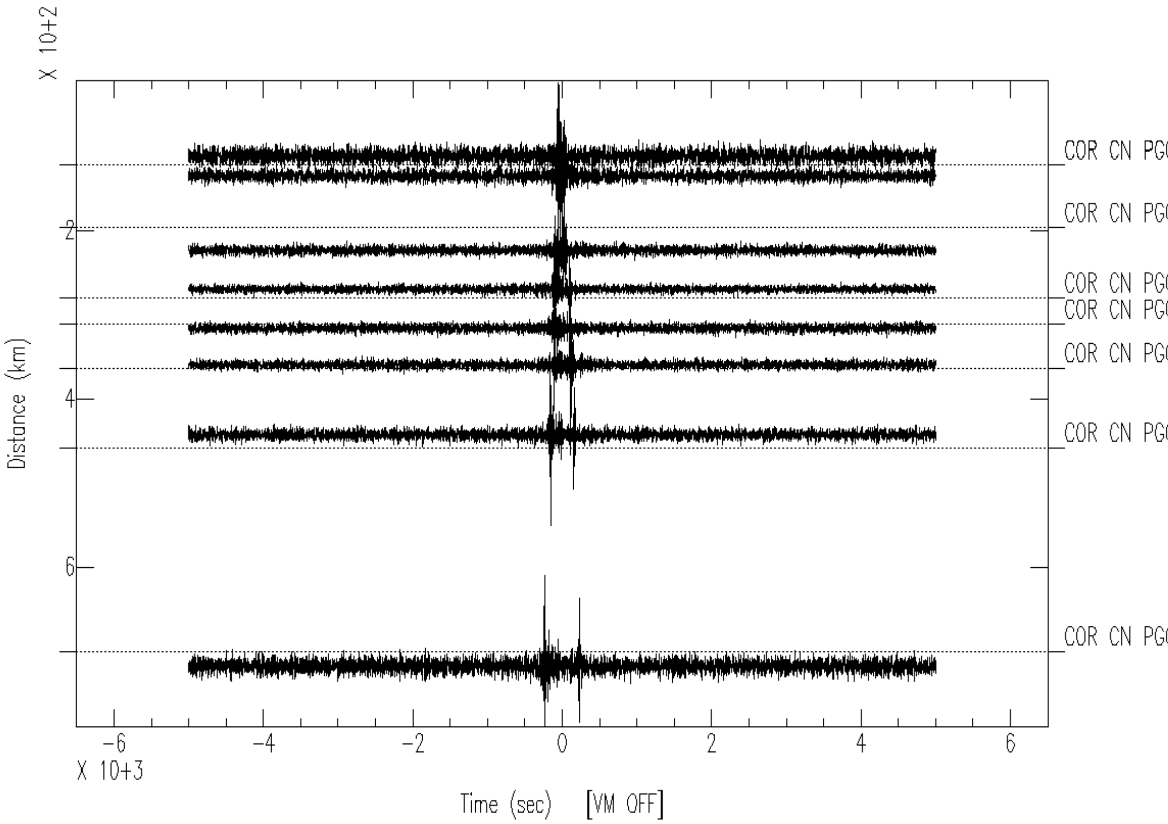

Figure 5.2: Cross-correlation record section for eight station pair. The traces are sorted by increasing interstation distance, ranging from approximately 110 to 700 km. The x-axis shows lag time in seconds (±6000 s), and the y-axis shows interstation distance in km. A prominent zero-lag spike is visible at $t = 0$ s, while surface wave energy appears on both the causal (positive lag) and acausal (negative lag) sides of the correlograms, consistent with Rayleigh wave propagation. The moveout of these arrivals with increasing distance illustrate the propagation of Rayleigh wave energy between station pairs.

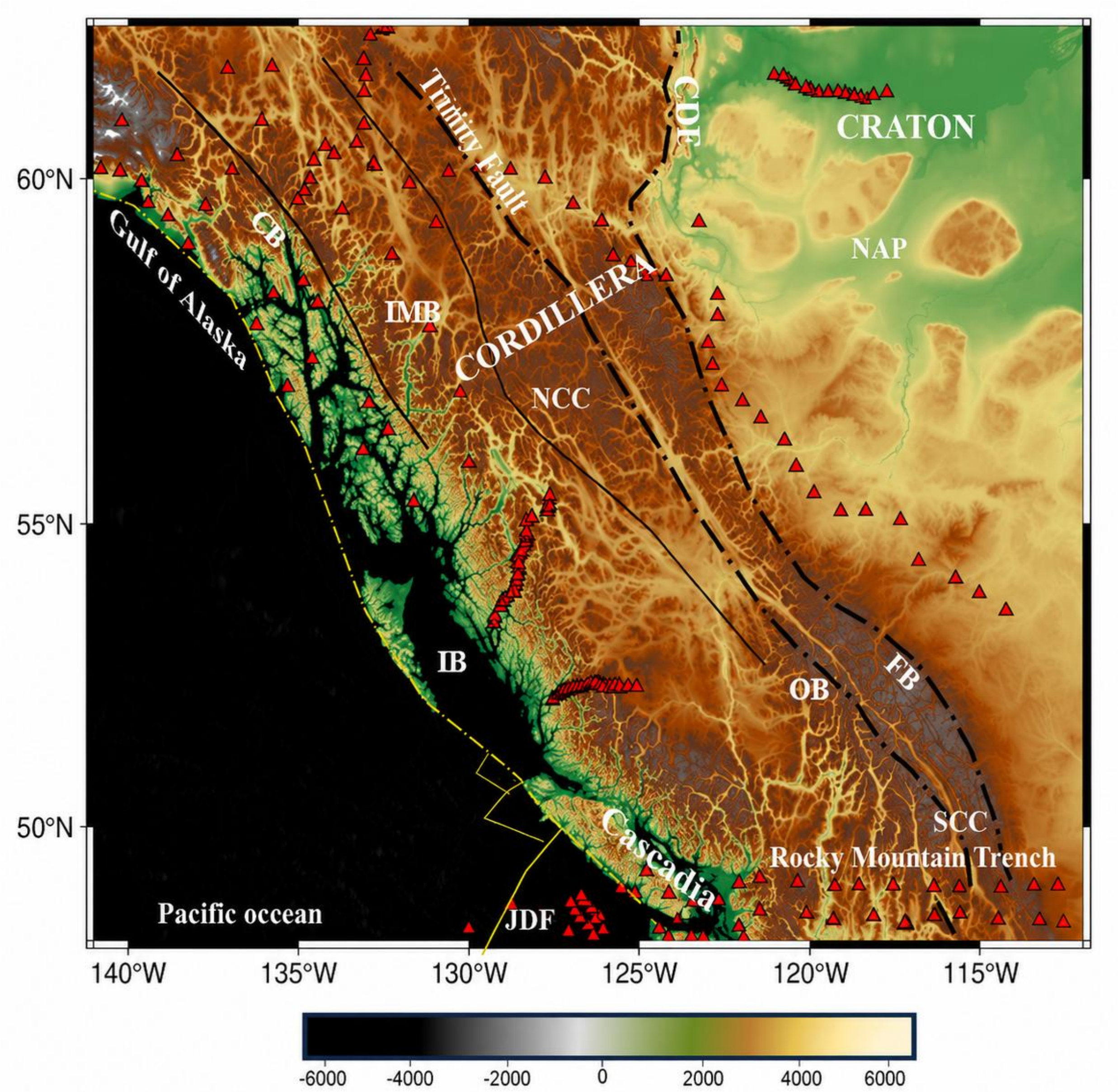

Figure 5.3: Topography map in western Canada. The Canadian Cordillera can be divided into the Northern Canadian Cordillera (NCC) and the Southern Cordillera (SCC). CDF is the Cordilleran Deformation Front; NAP is the North American Plate; JdF is the Juan de Fuca Plate; Red triangles indicate the seismograph station. Black and yellow lines mark major tectonic structures in western Canada. (Nelson et al., 2013). The Cordillera is divided into distinct morphologic belts: Insular Belt [IB], Coast Belt [CB], Intermontane Belt [IMB], Omineca Belt [OB], and Foreland Belt [FB] (Gabrielse and Yorath, 1992).

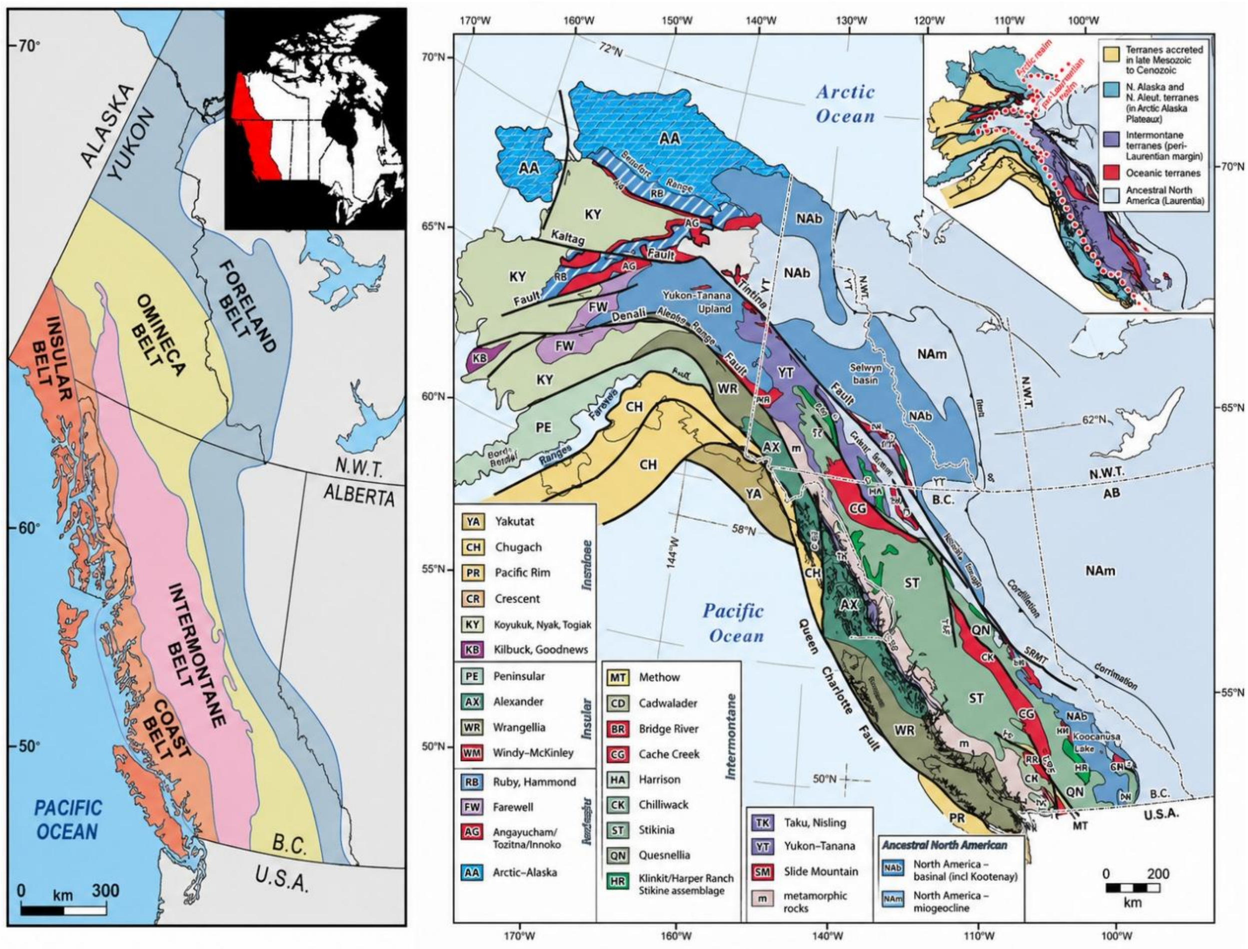

Figure 5.4: Geological terrane map of western Canada and Alaska, modified after Nelson et al. (2013). The left panel shows the major morphotectonic belts of the Canadian Cordillera, including the Insular, Coast, Intermontane, Omineca, and Foreland belts, and their position relative to the cratonic interior. The right panel provides a more detailed terrane map showing accreted crustal blocks, including Wrangellia, Stikinia, Yukon-Tanana, Cache Creek, Quesnellia, Chugach, Alexander, and related terranes, together with major fault systems and terrane-bounding structures. In this study, the terrane framework is used to compare the observed seismic velocity variations with known geological boundaries, particularly across the Cordillera-craton transition, the Intermontane Belt, the Insular Belt, and major fault zones such as the Tintina Fault and Rocky Mountain Trench.

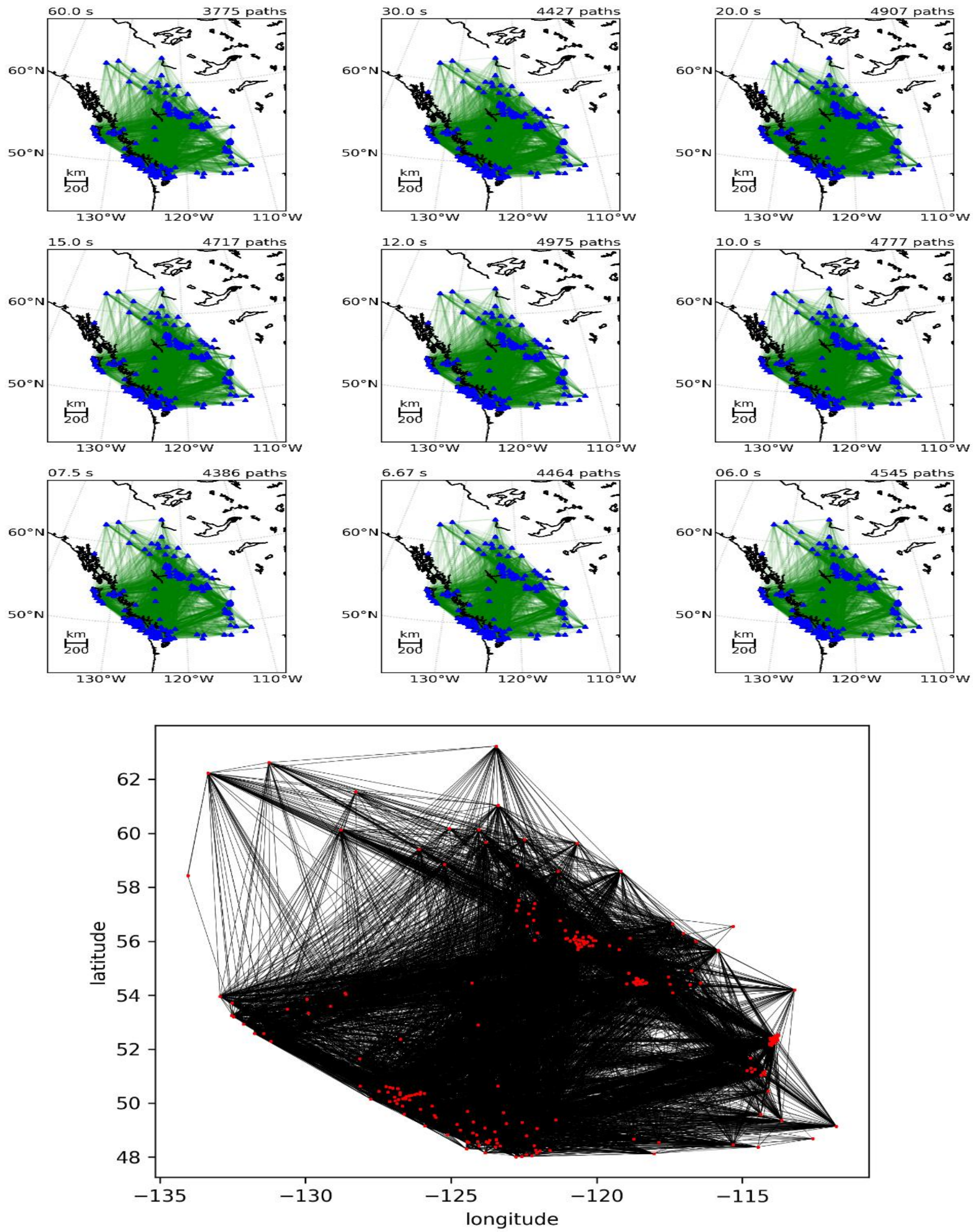

Figure 5.5a: Ray-path coverage for the Rayleigh wave phase velocity measurements used in this study.

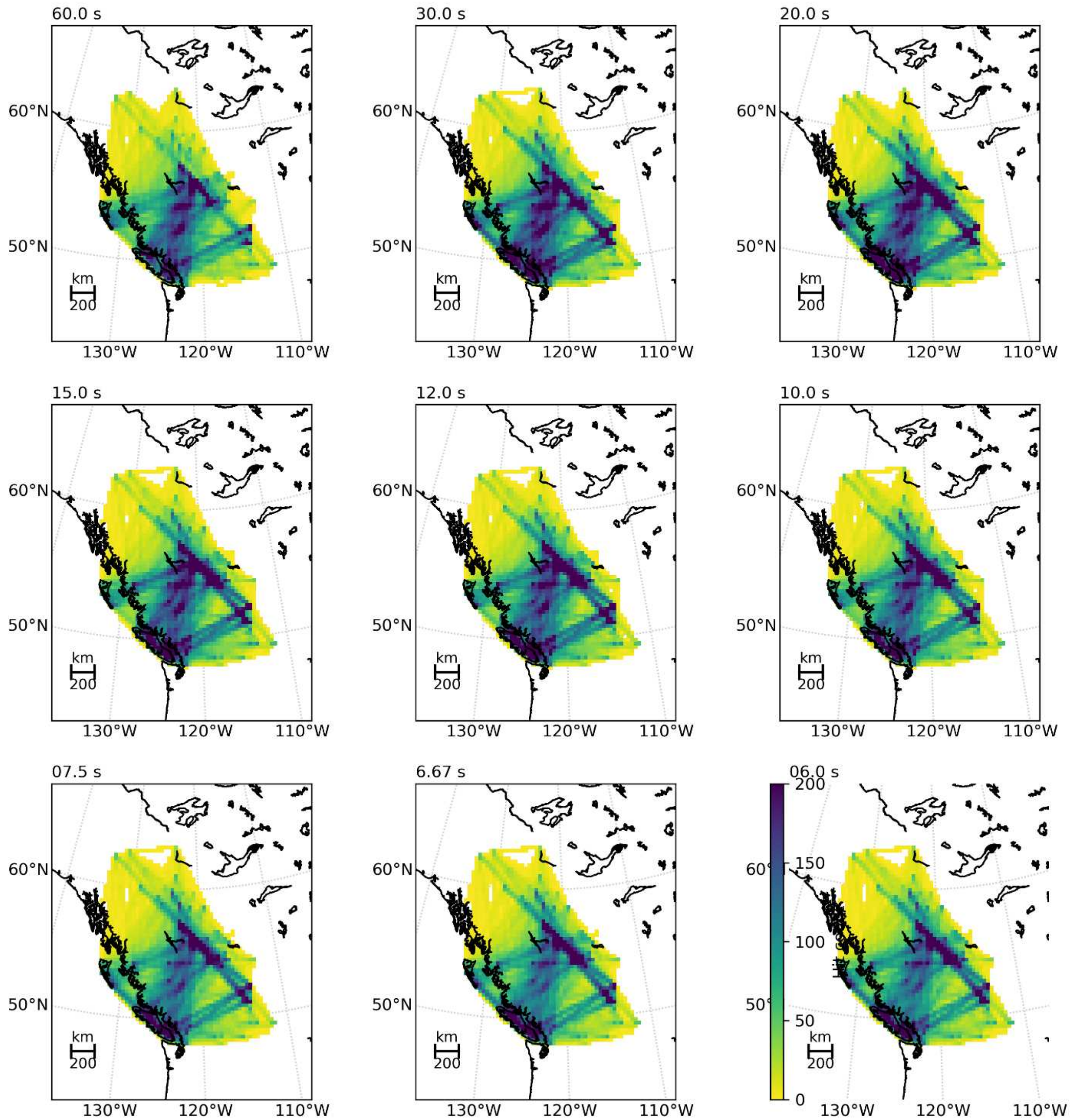

Figure 5.5b: Seismic ray-path hit-count maps for Rayleigh wave phase velocity measurements at periods from 6.0 to 60.0 s across western Canada. Each panel shows how frequently different parts of the study area are sampled by interstation paths at a given period. Darker purple colors indicate higher hit counts and denser ray coverage, while yellow colors indicate lower hit counts and weaker sampling. The maps show that ray coverage is strongest across the central part of the study area, where the tomographic results are better constrained, and become weaker toward the outer margins.

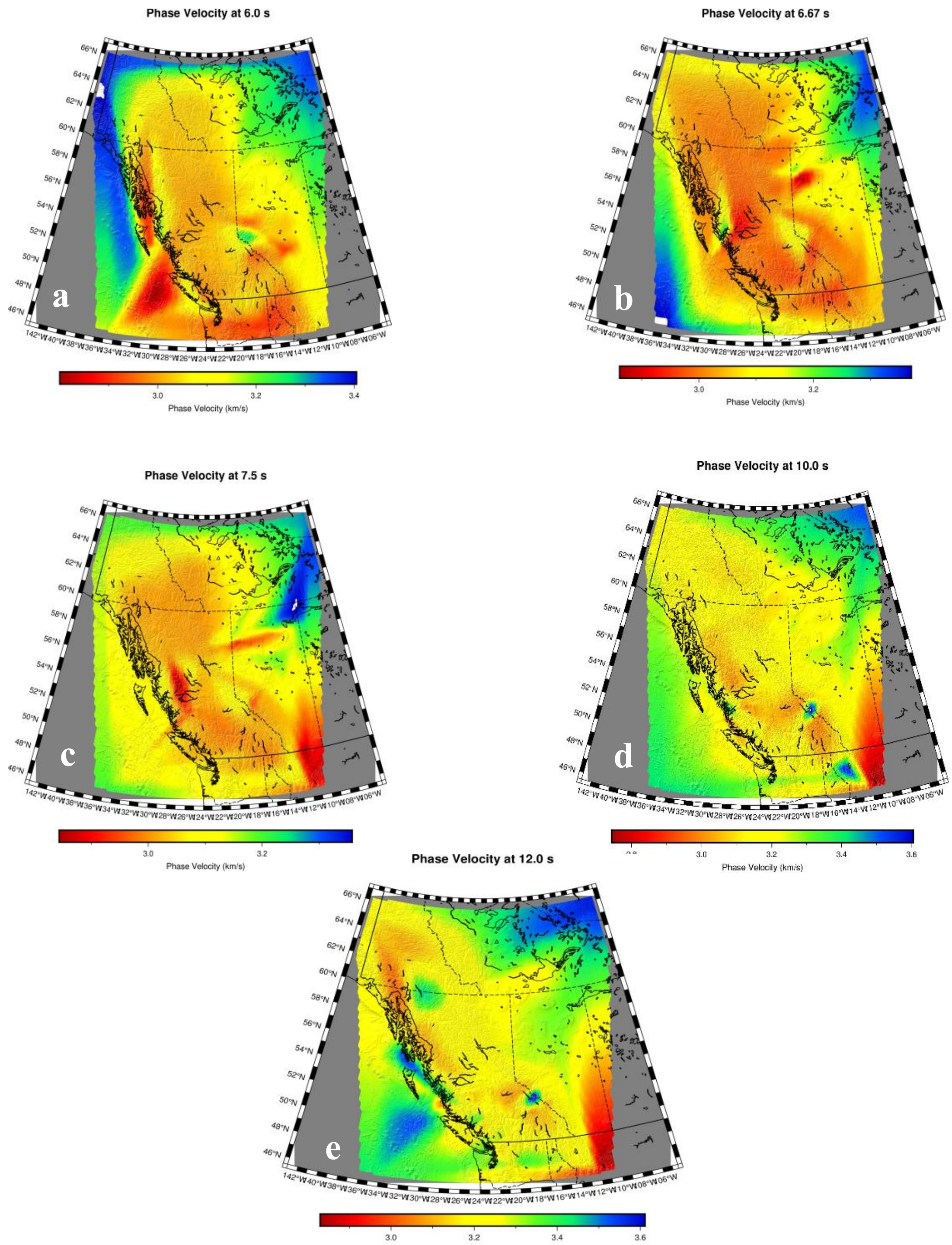

Figure 5.6a: Phase velocity maps at periods of (a) 6.0 s, (b) 6.67 s, (c) 7.5 s, (d) 10.0 s, and (e) 12.0 s across western Canada. Red and blue colors indicate low and high phase velocities, respectively. The persistent low-velocity anomaly along the western margin reflects the tectonically active Cordillera, while the high-velocity region in the northeast is associated with the stable Canadian Shield craton.

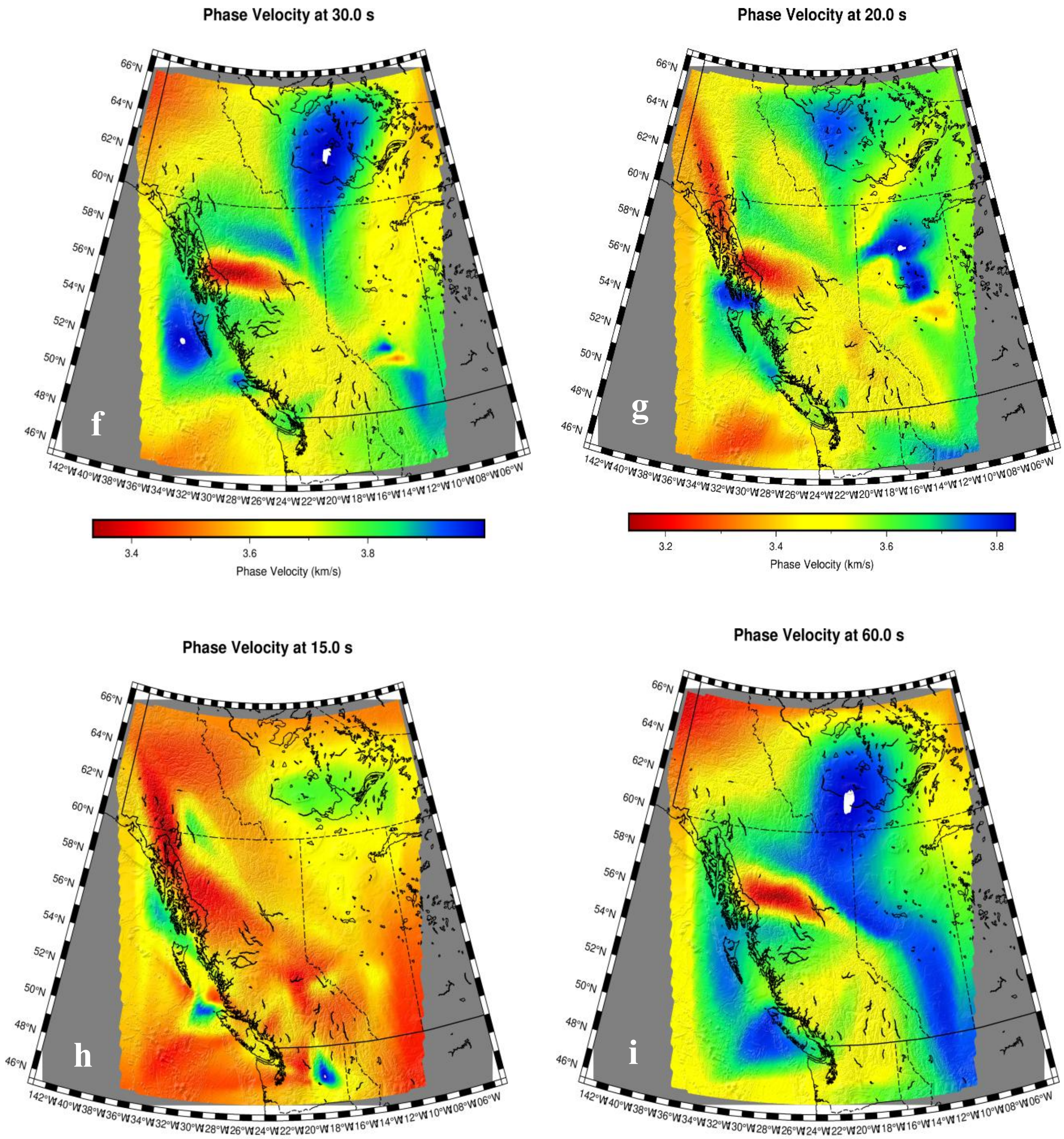

Figure 5.6b: Phase velocity maps at periods of (f) 30.0 s, (g) 20.0 s, (h) 15.0 s, and (i) 60.0 s across western Canada. Red and blue colors indicate low and high phase velocities, respectively. Overall, Panels (a-i) show how phase velocity changes across different periods, revealing a consistent velocity contrast between the tectonically active Cordillera. in the west and the stable craton in the northeast.

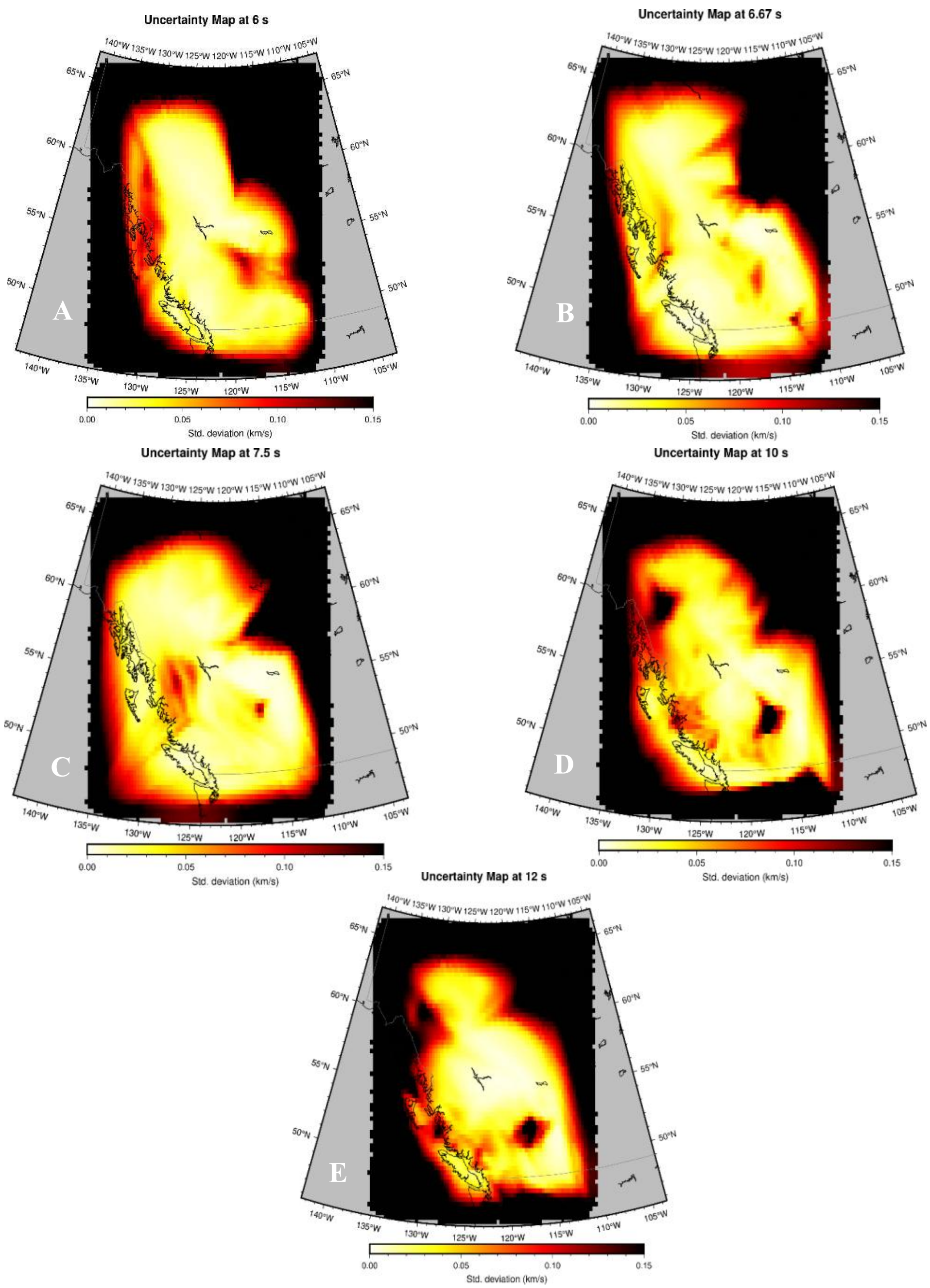

Figure 5.7a: Uncertainty maps of phase velocity estimates for western Canada at periods of (A) 6.0 s, (B) 6.67 s, (C) 7.5 s, (D) 10.0 s, and (E) 12.0 s. The color scale represents the standard deviation of phase velocity in km/s. Lighter yellow to white areas indicate lower uncertainty and better-constrained velocity estimates, while red to black areas indicate higher uncertainty or poorly constrained regions. The lowest uncertainties are mainly concentrated within the central part of the study area, whereas higher uncertainties occur toward the margins and in areas with weaker data coverage.

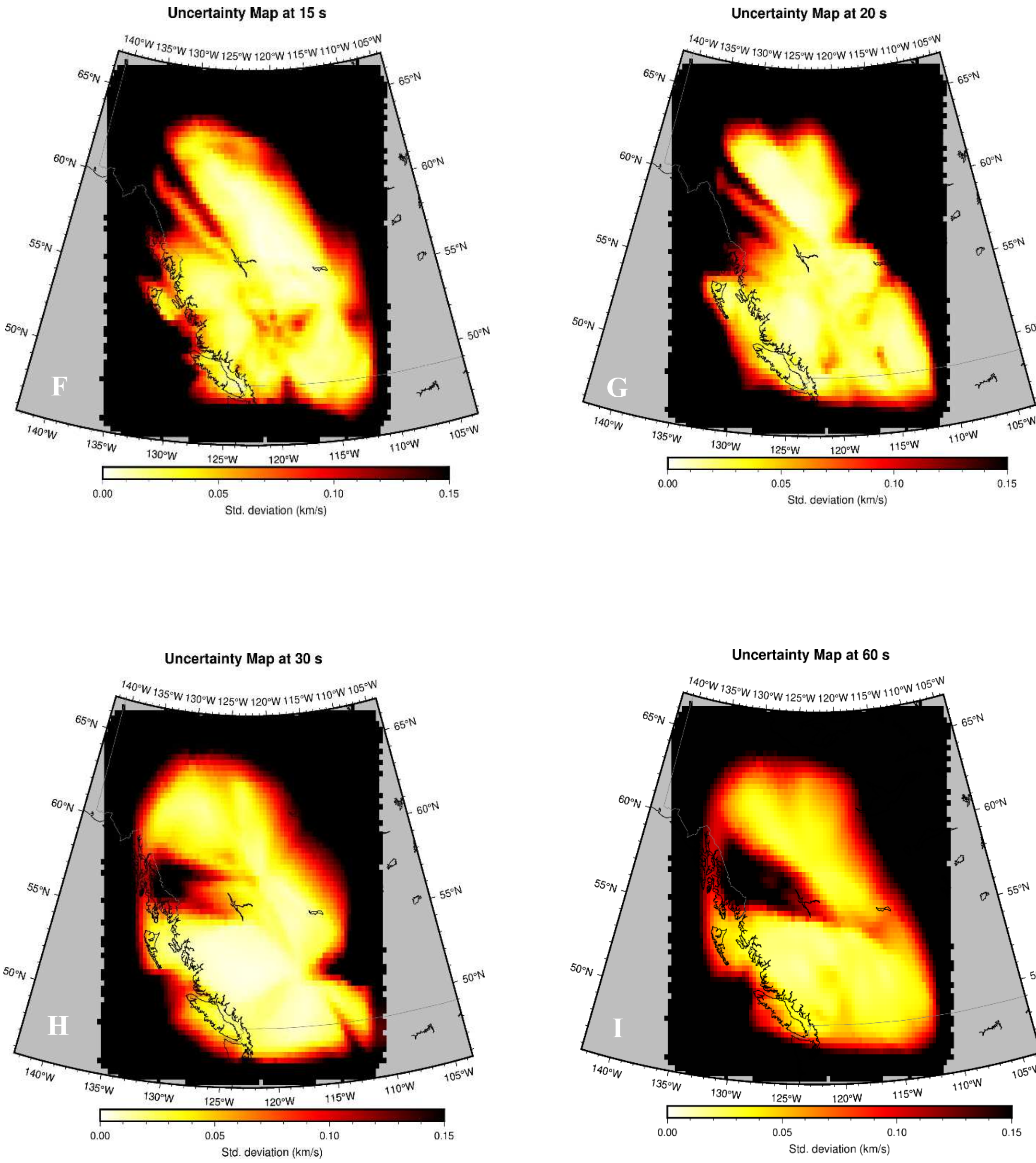

Figure 5.7b: Uncertainty maps of phase velocity estimates for western Canada at longer periods of (F) 15.0 s, (G) 20.0 s, (H) 30.0 s, and (I) 60.0 s. The color scale represents the standard deviation of phase velocity in km/s. Lower values indicate better-constrained velocity estimates, while higher values indicate less reliable areas. Overall, uncertainty is relatively lower across the main Cordilleran and adjacent foreland region, where the velocity estimates are better constrained, while uncertainty increases toward the cratonic side and the outer margins of the study area, especially at longer periods.

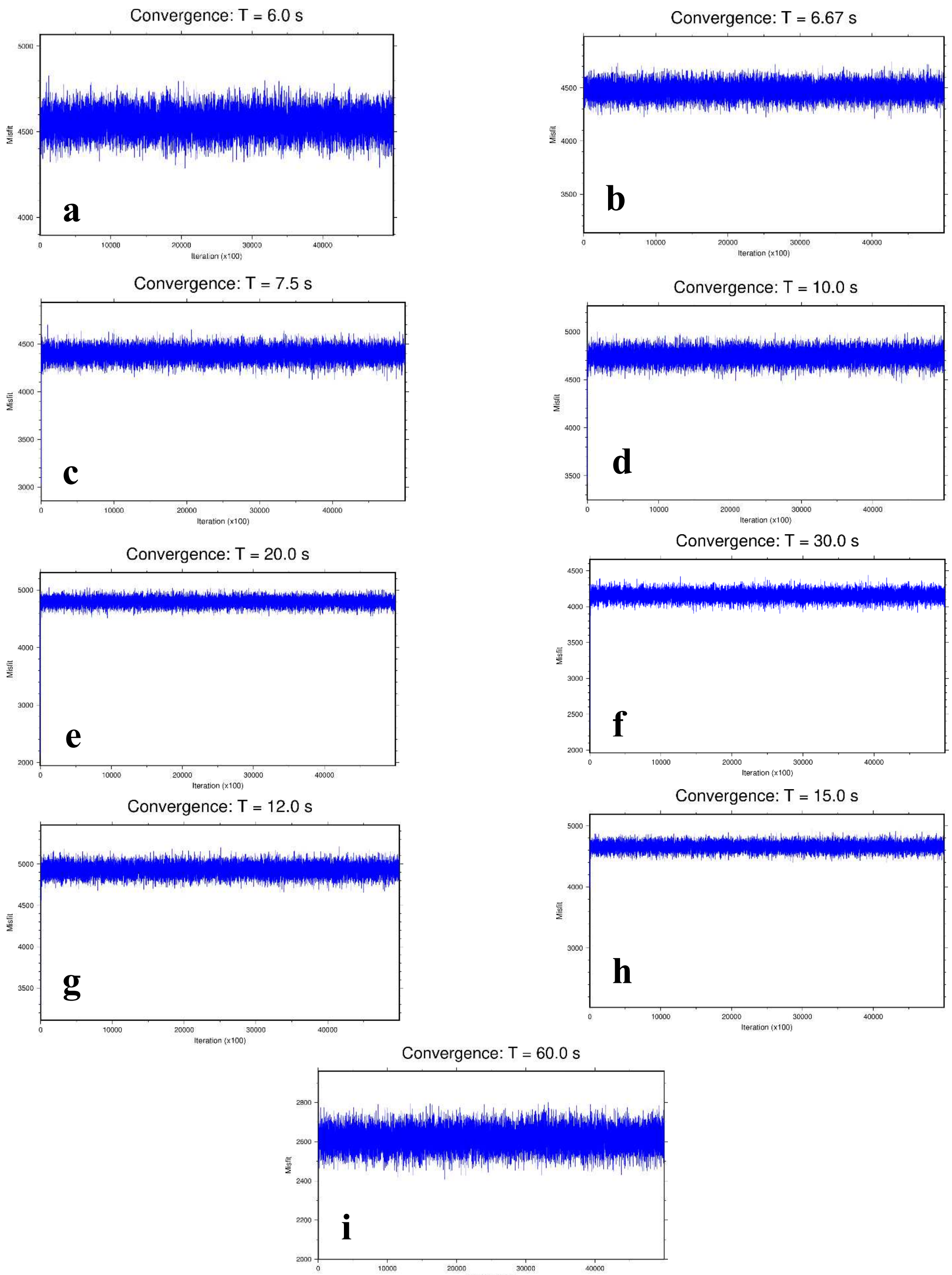

Figure 5.8: Convergence curves for the phase velocity inversion at periods of (a) 6.0 s, (b) 6.67 s, (c) 7.5 s, (d) 10.0 s, (e) 20.0 s, (f) 30.0 s, (g) 12.0 s, (h) 15.0 s, and (i) 60.0 s. Each panel shows the change in mean squared error (MSE) with iteration number. For all periods, the MSE remains within a stable range after the early iterations, indicating that the inversion achieved stable convergence.

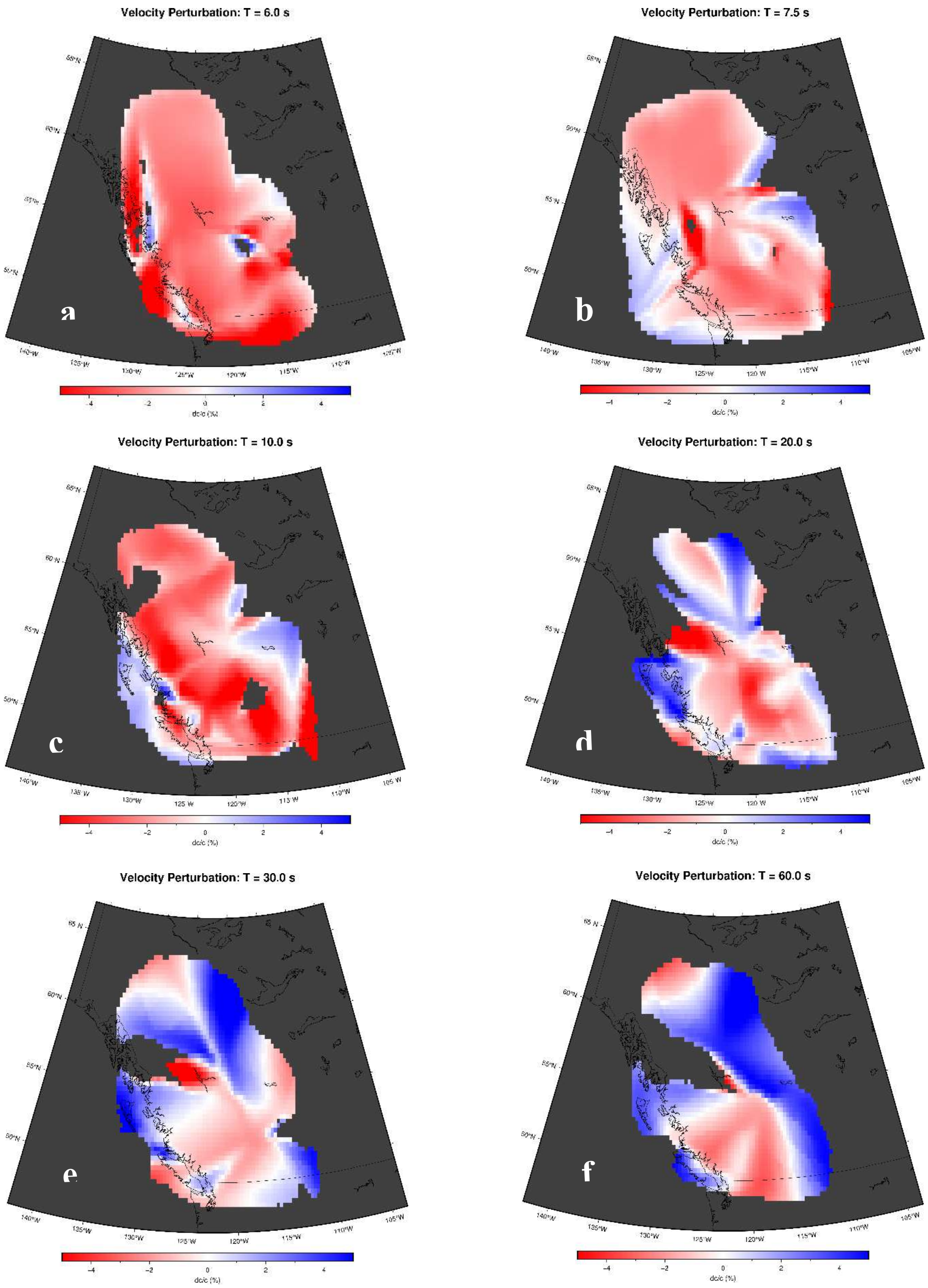

Figure 5.9: Velocity perturbation maps for western Canada at periods of (a) 6.0 s, (b) 7.5 s, (c) 10.0 s, (d) 20.0 s, (e) 30.0 s, and (f) 60.0 s. The perturbations are expressed as dc/c (%) relative to the reference phase velocity at each period. Red colors indicate negative velocity perturbations, blue colors indicate positive velocity perturbations, and white colors represent values close to zero. The maps were masked using the corresponding uncertainty maps, and gray regions indicate poorly constrained areas where the standard deviation exceeds the selected uncertainty threshold; these regions are excluded from interpretation.

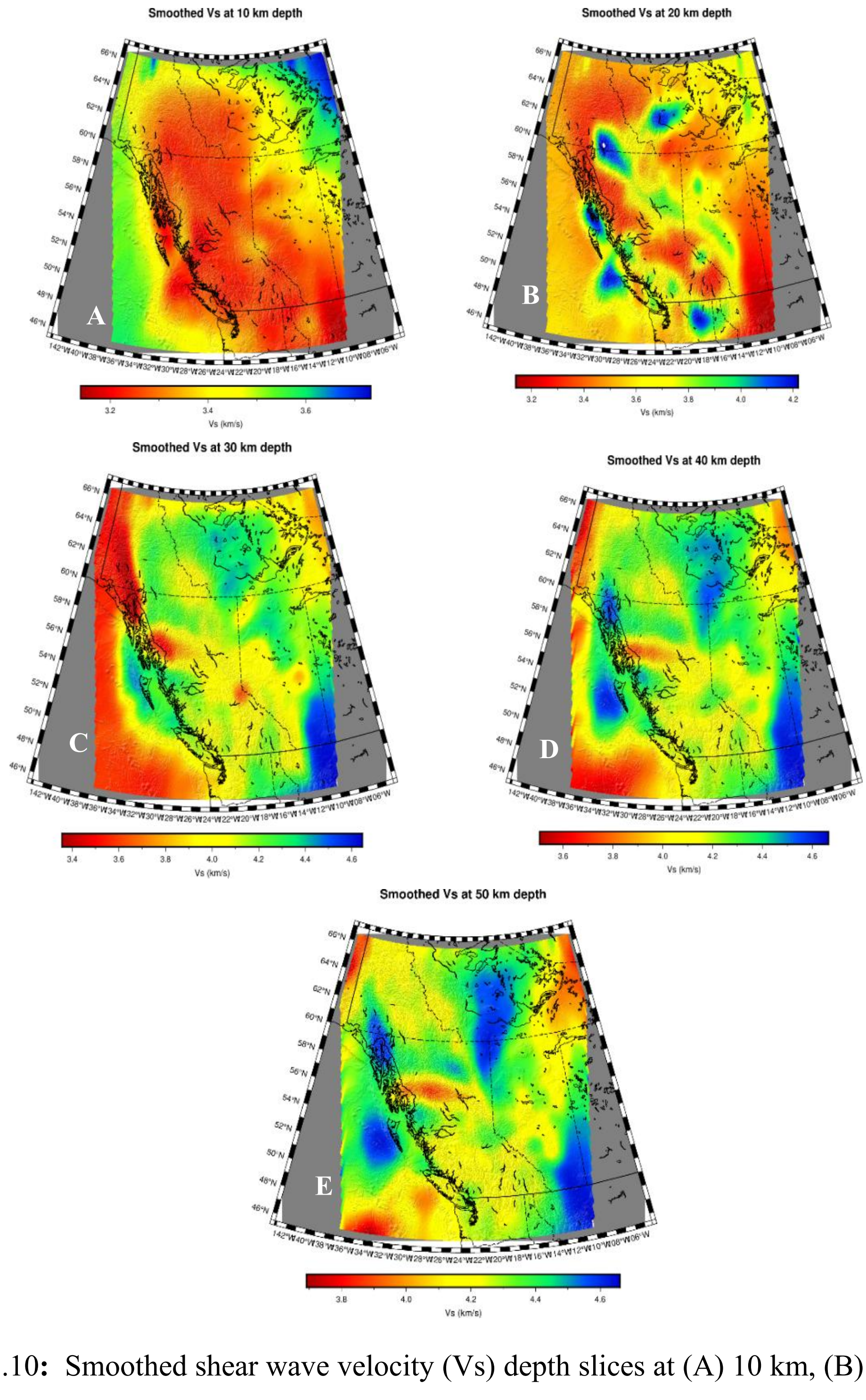

Figure 5.10**:** Smoothed shear wave velocity (Vs) depth slices at (A) 10 km, (B) 20 km, (C) 30 km, (D) 40 km, and (E) 50 km depth beneath western Canada. The color scale represents Vs in km/s, with red indicating low velocities and blue indicating high velocities. Low Vs values in the west correspond to the tectonically active Cordillera, while high Vs values in the northeast reflect the stable Canadian Shield craton.

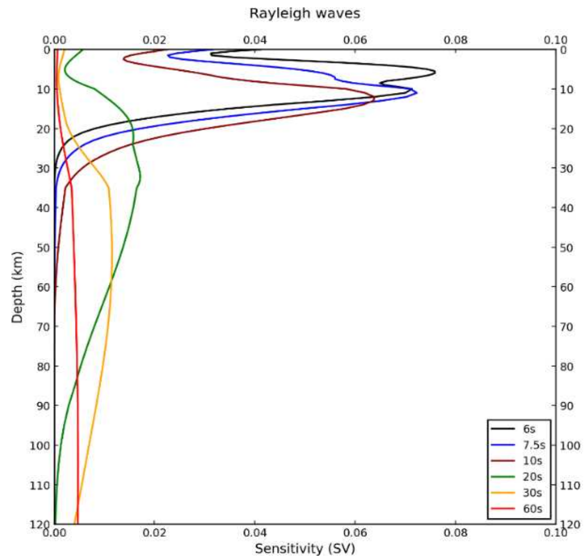

Figure 5.11: Rayleigh wave depth sensitivity kernels for periods of 6.0, 7.5, 10.0, 20.0, 30.0, and 60.0 s. The curves show how Rayleigh wave phase velocity is sensitive to shear wave velocity structure at different depths.

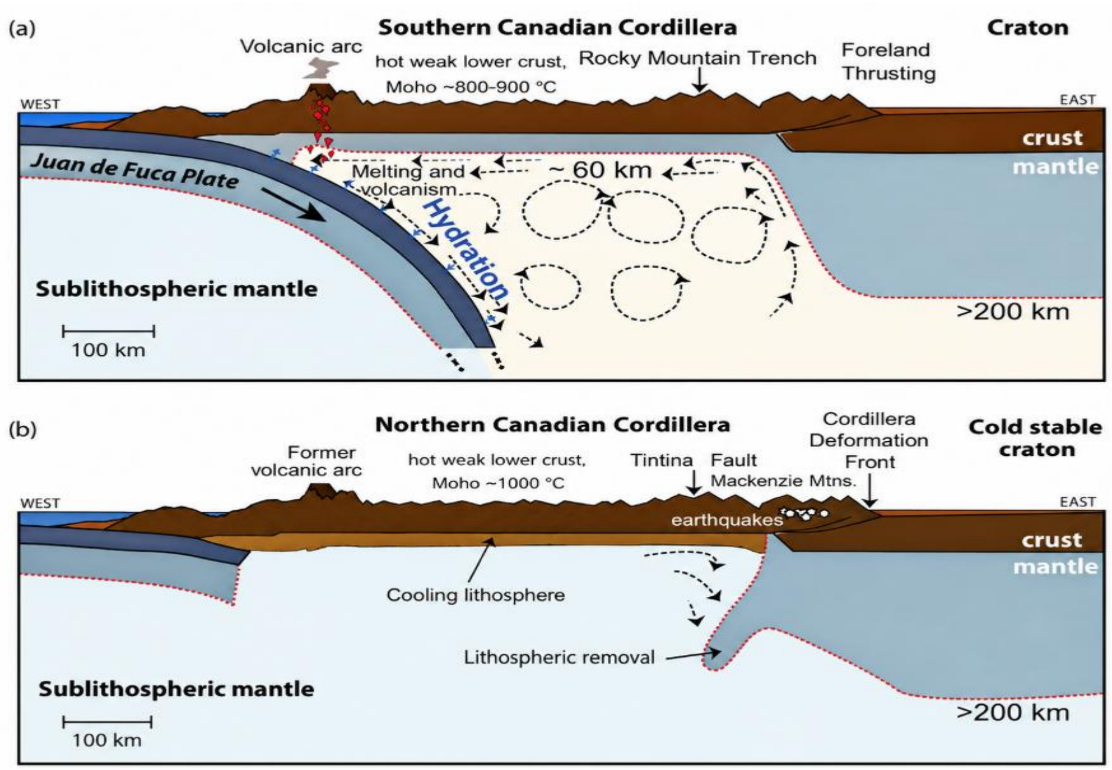

Figure 5.12: Conceptual models illustrating possible lithospheric evolution scenarios in western Canada. (a) Schematic representation of the Southern Canadian Cordillera. (b) Schematic representation of the Northern Canadian Cordillera. (Modified after Hyndman et al., 2005, and Audet et al., 2019).

```
1  5000000            ! Max number of iterations
2  100                ! How often to save model iteration
3  10                 ! Number of temp steps
4  1.02               ! Temp multiplicative factor
5  8                  ! Number of threads (if using OPENMP)
6  -151               ! Random number seed (must be negative)
7  2.0 4.0 0.1        ! Min, Max & sigma for parameter # 1 (Group or Phase velocity in km/s)
8  0                  ! Use input errors (1) or estimate 'a' and 'b' parameters (0)
9  0.0 0.01 0.0001    ! Min, Max & sigma for error parameter 1 (a value - not used if ablve is set to 1)
10 0.0001 3.0 0.01    ! Min, Max & sigma for error parameter 2 (b value - not used if above is set to 1)
11 0.0 15.0 5.0       ! Min, Max & sigma for node movement (scaled by number of integration grid cells)
12 5 500              ! Min, Max number of nodes
13 /home/jeremyg/Data/CascadiaVIHG/Taylor/topo_ice_matrix.txt
14 30.0               ! Map gridspacing (km)
15 /home/jeremyg/Data/CascadiaVIHG/Taylor/PATHS/
16 3318               ! Number of path files in dataset
17 15.0               ! Desired period for inversion
18 100                ! Cutoff (Burn-in samples to exclude from post-processing - relative to how many iterations are saved)
19
```

Figure 5.13: Screenshot of the script “tomo_input.dat”.

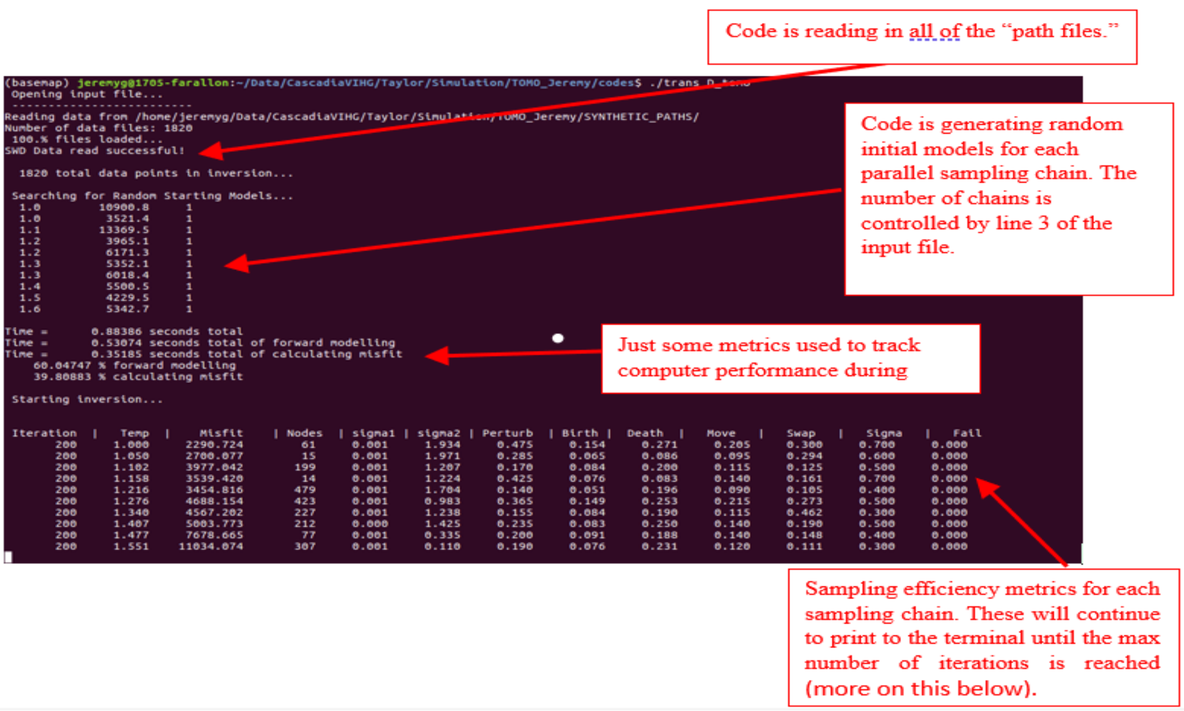

Figure 5.14: Screenshots of running trans_D_tomo code. This screenshot shows the execution of the trns_D_tomo script, which reads in all the necessary "path files" and generates random initial models for each parallel sampling chain.

Appendix I

Data Processing Sequence

This research is conducted in two steps: Step 1 is data collection and Step 2 is tomographic inversion. All the necessary scripts for Steps 1 and 2 are accessed on a remote server via ssh. These scripts are in the directory:/data/geo/seismo/Research/w_Canada_ambient/scripts/

The key scripts for Step 1 include:

- run_LHZ_wCanada.tcsh
- run_BHZ_wCanada.tcsh
- run_LHZ_BHZ_wCanada.tcsh

These scripts are well-documented and designed to execute Step 1 efficiently. They prompt the user to adjust relevant parameters before running. After executing, the resulting data files are stored in: /scratch/derek_wCanada/Data/LHZ_BHZsm/AMP_DISP.

For Step 2, the tomalika_tomography folder within the same directory contains all the necessary scripts for the ambient noise tomography code, which is used during the inversion process.

STEP 1: This study's data collection process focuses on acquiring and processing seismic data for ambient noise tomography in western Canada. The following sections outline the steps to gather and prepare the data for the analysis using scripts such as run_LHZ_BHZ_wCanada.sh, run_LHZ_wCanada.sh, and run_BHZ_wCanada.sh to ensure consistency in data processing across different channels and components.

1. **Seismic Data Acquisition**: The region of interest for this project spans from latitude 48°N to 62°N and longitude 112°W to 141°W, covering the southern portion of western Canada. The period of interest ranges from January 2000 to June 2024. Day-long vertical-component seismograms are downloaded from all available stations within the defined region using data from

the Incorporated Research Institutions for EarthScope DMC to collect the seismic data. The first step in the data collection process involves the following steps:

- **Download seismic data:** Shell scripts are employed to download the seismic data, where data directories are defined to ensure proper organization.The scripts prep_ant_data_LHZ.tcsh, prep_ant_data_BHZ.tcsh. and prep_ant_data_LHZ_BHZ.tcsh gathers seismic data for the specified latitudinal and longitudinal bounds and periods.
- **Data organization**: The seismic data is stored in the designated directory run_LHZ_BHZ_wCanada.tcsh, ensuring all available station data is organized for subsequent processing.

2. Data Preparation: Once the seismic data is collected, it undergoes several preprocessing steps to condition the data for analysis:

- **Data conditioning:** This involves removing mean and trend from the data, tapering, and eliminating the instrument response. Spectral whitening is applied to enhance the signal quality.
- **Cross-correlation:** To extract useful seismic signals, the seismic waveforms for all available station pairs are cross-correlated. The cross-correlated data is stored in the COR directory.
- **Stacking:** Monthly correlations between station pairs are stacked to increase the signal-to-noise ratio (SNR), improving the signals' clarity. The stacking process is managed using the run_stack_rp_2. tcsh script, which compiles station-station correlations into a single dataset.

3. Data Cleanup: During the correlation process, some directories may contain incomplete or invalid data. These are removed to ensure only high-quality data is retained:

- **Removal of invalid data:** Any directories containing incomplete header information or no data are removed. The cleanup process is automated using the script find_bad_files.tcsh.

- **Averaging correlations:** The positive and negative parts of the correlations are averaged to create a more symmetric dataset, further improving data quality.

4. Group and Phase Velocity Measurement: After cleaning and averaging the data, group, and phase velocity measurements are extracted from the symmetric correlation data:

- **Velocity measurement:** The run_ftan.bash script computes group and phase velocities for the processed data. These velocity measurements are stored in DISP and AMP files, representing dispersion and amplitude data.
- **Selection based on SNR (Signal-to-Noise Ratio):** Only those with sufficient SNR are selected for further analysis to ensure reliable measurements. This process is handled by run_select_dispersion_phase.tcsh and run_select_dispersion_group.tcsh scripts, which analyze the phase and group velocity data based on the SNR.

5. Data Archiving: Finally, all processed data, including the stacked correlations, velocity measurements, and cleaned files, are organized into their respective directories for later use in tomography analysis:

- **Archiving:** The processed data is moved to the appropriate directories, such as SAC, AMP_DISP,lists and SELECT, ensuring that all relevant data is easily accessible for further analysis.

This systematic data collection process ensures that only high-quality seismic data is used in the subsequent tomography analysis, providing a solid foundation for producing high-resolution images of the lithospheric structure in western Canada. Here, High-quality data in this context refers that exhibit a high signal-to-noise ratio (SNR), minimal instrumental noise, and complete daily records without gaps or errors. The collected data will be used in the inversion process to obtain the final tomography models.

STEP 2: For the second step of our research, the data processing is carried out using specific scripts and instructions designed by Jeremy Gosselin. The process involves refining and preparing the raw data for the tomography inversion, as detailed below.

1. Data Sorting and Preparation for Inversion

- First, set up a new Anaconda environment and make sure all dependent libraries (pandas, matplotlib, numpy, os, basemap, scipy, obspy, shapely, mpl_toolkits, datetime, fnmatch) are available in this Anaconda environment.
- Then, the script Data_sort.py is used to search through the contents of the "SELECT" directory. This directory contains all the dispersion files collected from STEP 1 for the study. The script removes data outside the defined study area, ensuring that only relevant data remains for further processing. Moreover, it removes multiple entries within the dataset, effectively cleaning the data for accurate analysis. After completing this sorting process, the script creates a new subdirectory that saves all the reformatted data. This process typically results in around 6662 data files.
- Following data sorting, the Tomo_map.py script reads the newly reformatted data files. The script performs outlier analysis to remove any erroneous or suspicious data points that could affect the results. Once the good data is identified, the script calculates all the necessary path information, which is crucial for the tomography inversion process. Therefore, the script generates several figures that visualize the path data. The output "path" files are then stored in the "PATH" directory, which the tomography inversion will later utilize. After this process, around 4,000 data files remain for the inversion stage. Also, the topo_ice_matrix.txt file, created by tomo_map.py, is generated for subsequent steps. It generates some figures like path coverage.png [Figure 5.5a], outlier_map.png, Final dataset.png, etc.

2. Running Tomographic Inversion

- In the Tomo_Inversion/codes directory, we have a collection of FORTRAN (.f90 or .f) files, which are the source code for the tomography inversion.

  Next, type:

make clean

Then:

make into the terminal while in the "Tomo_Inversion/codes" directory. This compiles the Fortran codes and produces two executables: trans_D_tomo and grid_models.

- The first executable is the reversible jump tomography code that generates samples from a posterior distribution. The second executable takes these samples calculates some basic statistics, and outputs a final model solution with uncertainty estimates onto a grid.
- Run the inversion code directly from the "Tomo_Inversion/codes" directory. However, it could be easier to stay organized by simply copying the executables into a new working directory. So, copy trans_D_tomo and grid_models from the Tomo_Inversion/codes directory into the Tomo_Inversion/working directory. NOTE: The working directory must have an empty sub-directory called results.
- In Tomo_Inversion/working, we now have a file called tomo_input.dat. This file contains all the control parameters for the reversible jump sampling [Figure 5.13]. For details, see publications (Bodin et al., 2009 and 2012; Gosselin et al., 2021).
- Some introductory comments on the various control parameters are included. For now, the most important is to update lines 13, 15, and 16 according to your system. Specifically,
    - Line 13 should point to the file topo_ice_matrix.txt, (Do not worry about this file– it is generated by the same python script that created the original "path'' files).
    - Line 15 should point to the PATHS directory that contains our simulated dataset (as discussed above).
    - Line 16 should be set to the number of files in the PATHS directory.
    - Line 5 is the number of CPU cores you wish to use. Edit this according to your computer system resources.
- Then, the machine is ready to run the inversion. Since the code takes so long to run, I recommend using the "nohup" function in Linux (or something similar) so that you can still have the code running in the background on your machine after closing the terminal [Figure 5.14].

Type:

./*trans_D_tomo* into the terminal. There are many things printed on the screen

- While the inversion is running, we will continue to see 13 columns of text printed to the terminal

To briefly explain these:

Iteration: is the number of samples produced by the algorithms so far (for all sampling chains). The inversion will continue to run until this reaches the maximum number of iterations specified in the input file (line 1).

Temp: is the "temperature" of the sampling chain (based on simulated annealing methodology). Only the Temp=1 sampling chain is unbiased and is used in the inversion output. However, the other chains can significantly aid overall algorithm efficiency by enabling chains to "swap" locations in the parameter space. Data misfit has less influence on higher temperature chains and so are not as easily trapped in local minima. See Gosselin et al. (2021) for details and additional references.

Misfit: This is the current model's data misfit for each sampling chain. Since data errors can fluctuate as part of the algorithm, we expect this misfit value to be approximately equal to the number of data (i.e., the number of input "path" files).

Nodes: The number of model nodes of the current model for each sampling chain. The nodes define a Delaunay triangulation and interpolation over the map area. The number and location of nodes are sampled as part of the problem. See Gosselin et al. (2021) for details and additional references.

Sigma1 and Sigma2: These are the data error parameters of the current model for each sampling chain. These are the 'a and 'b' parameters as defined in Gosselin et al. (2021).

Perturb, Birth, Death, Move, Swap, and Fail: are the percentages of accepted model changes for different types of operations. "Perturb" represents a perturbation to a parameter of the existing model. "Birth" and "Death" represent the addition or removal of nodes from the model. "Move" represents moving a node within the map space. "Swap" is when two parallel sampling chains swap location within the parameter space. "Fail" is when the forward calculation (travel-time prediction) numerically fails. Ideally, these metrics should be 10-70% (though birth/death metrics are often lower). The fail metric should be near zero.

- The input parameters can help adjust the algorithm efficiency, which these metrics record. This takes some trial-and-error for every problem/dataset.
- complete or has enough samples/iterations. For most problems, the inversion requires several million samples at a minimum (assuming the algorithm efficiency is correctly setup).
- We have now seen several large files in the Tomo_Inversion/working/results directory, most of which are in binary format to preserve computer storage space. These files contain various information on the models' ensemble from the sampling we just conducted. Type:

  ./grid_models

  into the terminal. This code runs very quickly (within a few seconds). It generates several text files containing the average model from the sampling and the standard deviation (among other things).
- We have a simple Python script that generates figures of the inversion output. These figures represent a guide for extracting the desired information from the inversion output. The script is plot_maps.py. It will generate a map of isotropic velocity and its uncertainty and histograms for the number of model nodes and the 'a' and 'b' data error parameters.
- Note that lines 151 and 296 in this script must point to the correct working directory.
- For the dataset and simulation parameters provided, we should retrieve a result similar to what is plotted [Figure 5.13 and Figure 5.14]

References

Adams, J., & Clague, J. J. (1993). Neotectonics and large-scale geomorphology of Canada. *Progress in Physical Geography: Earth and Environment*, *17*(2), 248-264. https://doi.org/10.1177/030913339301700209.

A. J. Wickens (1977). The upper mantle of southern British Columbia. *Canadian Journal of Earth Sciences*, *14(5)*: 1100-1115. https://doi.org/10.1139/e77-101.

A. J. Wickens and G. R. Buchbinder (1977). *S*-wave residuals in Canada. *Bulletin of the Seismological Society of America 1980; 70 (3)*: 809–822. doi: https://doi.org/10.1785/BSSA0700030809.

Audet, P., Currie, C., Schaeffer, A., and Hill, A. (2019). Seismic evidence for lithospheric thinning and heat in the northern Canadian Cordillera*. Geophysical Research Letters, 46*:4249–4257.

Baker, M. G., Heath, D. C., Schutt, D. L., Aster, R. C., Cubley, J. F., & Frey- mueller, J. T. (2019). The Mackenzie Mountains EarthScope Project: Studying active Deformation in the Northern North American Cordillera from margin to Craton. *Seismological Research Letters*. doi: 10.1785/0220190139

Bedle, H. & van der Lee, S. (2009). S velocity variations beneath North America. *J. Geophys. Res. Solid Earth 114*, B07308.

Behr, Y., J. Townend, S. Bannister, and M. K. Savage (2011). Crustal shear wave tomography of the 803 Taupo Volcanic Zone, New Zealand, via ambient noise correlation between multiple three-component networks, *Geochem. Geophy. Geosy., 12*, Q03015, doi:03010.01029/02010GC003385.

Bensen, G. D., M. H. Ritzwoller, M. P. Barmin, A. L. Levshin, F. Lin, M. P. Moschetti, N. M. Shapiro, and Y. Yang (2007). Processing seismic ambient noise data to obtain reliable broad-band surface wave dispersion measurements, *Geophys. J. Int., 169*, 1239-1260, doi: 1210.1111/j.1365-1246X.2007.03374.x.

Bensen, G. D., M. H. Ritzwoller, and N. M. Shapiro (2008). Broadband ambient noise surface wave tomography across the United States, *J. Geophys. Res., 113*, B05306, doi:05310.01029/02007JB005248.

Bensen, G. D., M. H. Ritzwoller, and Y. Yang (2009). A 3-D shear velocity model of the crust and uppermost mantle beneath the United States from ambient seismic noise, *Geophys. J. Int., 177(3)*, 1177-1196.

Bodin, T. & Sambridge, M., (2009). Seismic tomography with the reversible jump algorithm, *Geophys. J. Int., 178(3)*, 1411–1436

Bostock, M. G., et al. (2012). Nature of the Low Velocity Zone in Cascadia From Receiver Function Waveform Inversion, *American Geophysical Union*, T22D-08.

Burchfiel, B. C., & G. A. Davis (1975). Nature and controls of Cordilleran orogenesis, western United States: Extensions of an earlier synthesis, *American Journal of Science*, *275-A*, 363-396.

Cassidy, J. F. (1995), Review: Receiver function studies in the southern Canadian Cordillera, *Can. J. Earth Sci., 32*, 1514-1519.

Chen, Y., Gu, Y. J., Currie, C. A., Johnston, S. T., Shu-Huei, H., Schaeffer, A. J., & Audet, P. (2019). Seismic evidence for a mantle suture and implications for the origin of the Canadian Cordillera. *Nature Communications, 10*, 2249.

Chulick, G. S., and W. D. Mooney (2002). Seismic structure of the crust and uppermost mantle of North America and adjacent oceanic basins: A synthesis. *Bulletin of the Seismological Society of America, 92*(6), 2478-2492.

Clowes, R. M., Zelt, C. A., Amor, J. R., & Ellis, R. M. (1999). Lithospheric structure in the southern Canadian Cordillera from a network of seismic refraction lines. *Canadian Journal of Earth Sciences*.,*36(11),* 1923–1947.

Cook, F. A., M, C. R., B, S. D., van der Velden, A. J., Hall, K. W., Erdmer, P., and Evenchick, C. A. (2004). Precambrian crust beneath the Mesozoic northern Canadian cordillera discovered by lithoprobe seismic reflection profiling. *Tectonics.*

Dalton, C. A., Gaherty, J. B., & Courtier, A. M. (2011). Crustal VS structure in northwestern Canada: Imaging the Cordillera-craton transition with ambient noise tomography. *J. Geophys. Res.: Solid Earth*, *in 116(12)*, 1-30. https://doi.org/10.1029/2011JB008499.

DeMets, C., and T. Dixon (1999**)**. New kinematic models for Pacific–North America motion from 3 Ma to present: Evidence for steady motion and biases in the NUVEL-1A model, in The Eastern Pacific Ocean and Hawaii-The Geology of North America N, edited by D. M. Christie-Blick and H. Morris, *Geological Society of America, Boulder, Colo.*, pp. 21–72, https://doi.org/10.1130/DNAG-GNA-N.21.

Eaton, D. W., Frederiksen, A. W., & Miong, S. K. (2005). Seismic evidence for convection-driven motion of the North American plate. *Nature*, *436(7050)*, 201–204.

Estève, I., et al. (2021), Surface wave tomography of the northern Canadian Cordillera using earthquake Rayleigh wave velocities, *J. Geophys. Res.: Solid Earth, in press (1)*, 427444.

Finzel, E. S., Flesch, L. M., Ridgeway, K. D., Holt, W. E., and Ghosh, A. (2015). Surface motions and intraplate continental deformation in alaska driven by mantle flow. *Geophysical Research Letters, 42*:4350–4358.

Flück, P., R. D. Hyndman, and C. Lowe (2003). Effective elastic thickness Te of the lithosphere in western Canada, *J. Geophys. Res., 108(B9)*, 2430, doi:2410.1029/2002JB002201.

Fouch, M., D.E., J., VanDecar, J., van der Lee, S., The Kaapvaal Seismic Group, (2004). Mantle seismic structure beneath the Kaapvaal and Zimbabwe Cratons. *South African Journal Geology 107*, 33–44.

Frederiksen, A. W., M. G. Bostock, J. C. VanDecar, and J. F. Cassidy (1998). Seismic structure of the upper mantle beneath the northern Canadian Cordillera from teleseismic travel-time inversion, *Tectonophysics, 294*, 43-55.

Frederiksen, A., Bostock, M., & Cassidy, J. (2001). S-wave velocity structure of the Canadian upper mantle, *1*, 175 – 191.

Frederiksen, A. W., S.-K. Miong, F. A. Darbyshire, D. W. Eaton, S. Rondenay, and S. Sol (2007). Lithospheric variations across the Superior Province, Ontario, Canada: Evidence from tomography and shear wave splitting, *J. Geophys. Res., 112*, B07318, doi:07310.01029/02006JB004861.

Fulton, R. J. (1989), Quaternary Geology of Canada and Greenland: Maps, International Specialized Book Service Incorporated. Green, D. H., and A. E. Ringwood (1972), A comparison of recent experimental data on the gabbro garnet granulite-eclogite phase transition, *J. Geology, 80(3)*, 277-288. doi:210.1086/627731.

Gabrielse, H., & Yorath, C. J. (1992). Geology of the Cordilleran Orogen in Canada. *Geological Survey of Canada*, *Geology of Canada, No. 4*, 843.

G. Buchbinder and G. Poupinet (1977). P-wave residuals in Canada. *Canadian Journal of Earth Sciences*. *14(6)*: 1292-1304. https://doi.org/10.1139/e77-118.

Gosselin, J. M., Audet, P., Schaeffer, A. J., Darbyshire, F. A., & Estève, C. (2021). Azimuthal anisotropy in Bayesian surface wave tomography: Application to northern Cascadia and Haida Gwaii, British Columbia. *Geophysical Journal International, 224(3)*, 1724–1741. https://doi. org/10.1093/gji/ggaa561.

Grand, S. P., Van der Hilst, R. D., & Widiyantoro, S. (1997). High resolution global tomography: a snapshot of convection in the Earth. *Geological Society of America Today*, 7(4).

Hasterok, D., and D. S. Chapman (2007). Continental thermal isostasy: 2. Application to North America. *Journal of Geophysical Research: Solid Earth, 112*, B06415.

Hoffman, P. F. (1988). United Plates of America, the birth of a craton: Early Proterozoic assembly and the growth of Laurentia. *Annu. Rev. Earth Planet. Sci., 16*, 543–603.

Hyndman, R. D. (2017). Lower-crustal flow and detachment in the North American Cordillera: A consequence of Cordillera-wide high temperatures. *Geophysical Journal International, 209*(3), 1779-1794.

Hyndman, R. D., and C. A. Currie (2011). Why is the North America Cordillera high? Hot backarcs, thermal isostasy, and mountain belts, *Geology, 39(8)*, 783-786, doi:710.1130/G31998.31991.

Hyndman, R. D. (2010). The consequences of Canadian cordillera thermal regime in recent tectonics and elevation: a review. *Canadian J. of Earth Sciences, 47*:621–632.

Hyndman, R. D., P. Flück, S. Mazzotti, T. J. Lewis, J. Ristau, and L. Leonard (2005), Current tectonics 888 of the northern Canadian Cordillera, *Can. J. Earth Sci., 42*, 1117-1136, doi:1110.1139/E1105-1023.

Hyndman, R. D., and T. S. Lewis (1999). Geophysical consequences of the Cordillera-Craton thermal transition in southwestern Canada, *Tectonophysics, 306*, 397-422, doi:310.1016/S0040- 882 1951(1099)00068-00062.

Johnston, S.T., (2008). The Cordilleran ribbon continent of North America. *Annual Review of Earth and Planetary Sciences 36*, 495–530. doi: 10.1146/annurev.earth.36.031207.124331.

Kao, H., Behr, Y., Currie, C. A., Hyndman, R. D., Townend, J., Lin, F. C., et al. (2013). Ambient seismic noise tomography of Canada and adjacent regions: Part I. Crustal structures. *Journal of Geophysical Research: Solid Earth, 118*, 5865–5887. doi:10.1002/2013JB010535.

Kiwamu Nishida, Ryota Takagi & Akiko Takeo (2024). Ambient noise multimode surface wave tomography. *Progress in Earth and Planetary Science, 11*, 4.

Kong, Q., Trugman, D. T., Ross, Z. E., Bianco, M. J., Meade, B. J., & Gerstoft, P. (2019). Machine learning in seismology: Turning data into insights. *Seismological Research Letters*, *90*(1), 3-14.

Lewis, T. J., Hyndman, R. D., and Fluck, P. (2003). Heat flow, heat generation, and crustal temperatures in the northern Canadian cordillera: Thermal control of tectonics. *J. Geophys. Res., 108*.

Lin, F.-C., M. P. Moschetti, and M. H. Ritzwoller (2008). Surface wave tomography of the Western United States from ambient seismic noise; Rayleigh and Love wave phase velocity maps, *Geophys. 39 J. Int., 173(1)*, 281-298, doi:210.1111/j.1365-1246X.2008.03720. x.

McLellan, M., Schaeffer, A. J., & Audet, P. (2018). Structure and fabric of the crust and uppermost mantle in the northern Canadian Cordillera from Rayleigh-wave tomography. *Tectonophysics, 724–725*, 28–41, doi: 10.1016/j.tecto.2018.01.11

Mercier, J.-P., M. G. Bostock, J. F. Cassidy, K. Dueker, J. B. Gaherty, E. J. Garnero, J. Revenaugh, and G. Zandt (2009). Body-wave tomography of western Canada, *Tectonophysics, 475*, 480-492, doi: 410.1016/j.tecto.2009.1005.1030.

Monger, J. and Price, R. (2002). The Canadian cordillera: Geology and tectonic evolution. *Canadian Society of Exploration Geophysicists*, pages 17–36.

Nelson, J., Colpron, M., & Israel, S. (2013). The Cordillera of British Columbia, Yukon, and Alaska: Tectonics and metallogeny. *Seismological Research Letters*, 89(4), 13791384.

Plafker, George, Gilpin, L.M., and Lahr, J.C. (1994). Neotectonic map of Alaska, in Plafker, George, and Berg, H.C., eds., The Geology of Alaska: *Geological Society of America Decade of North American Geology*, *v. G-1*, 2 sheets, scale 1:2,500,000. Out of print, copy available online, http://dggs.alaska.gov/pubs/id/22261.

Ritzwoller, M. H., F.-C. Lin, and W. Shen (2011). Ambient noise tomography with a large seismic array, *Comptes Rendus Geoscience. 343.* 558-570, doi: 510.1016/j.crte.2011.1003.1007.

Rondenay, S., Bostock, M. G., & Shragge, J. (2000). Multiparameter two-dimensional inversion of scattered teleseismic body waves 3. Application to the Cascadia 1993 data set. *Journal of Geophysical Research: Solid Earth*, *105(B6)*, 30795 – 30807.

Ross, G. M., Parrish, R. R., Villeneuve, M. E. & Bowring, S. (1991). A. Geophysics and geochronology of the crystalline basement of the Alberta Basin, western Canada. *Can. J. Earth Sci. 28*, 512–522.

Sabra, K. G., P. Gerstoft, P. Roux, W. A. Kuperman, and M. C. Fehler (2005). Surface wave tomography from microseisms in Southern California, *Geophys. Res. Lett., 32(14)*, L14311, doi:14310.11029/12005GL023155.

Schaeffer & Lebedev (2014). Imaging the North American continent using waveform inversion of global and US Array data, *Earth-and-Planetary-Science-letters, Vol:402*, pages: 26-41, doi:10.1016/j.epsl.2014.05.014.

Sears, J. W. (2007). Belt–Purcell Basin: Keystone of the Rocky Mountain fold-and-thrust belt, U.S. and Canada, in *Whence the Mountains? Inquiries into the Evolution of Orogenic Systems: A Volume in Honor of Raymond A. Price*, edited by J. W. Sears, T. A. Harms, and

C. A. Evenchick, *Geological Society of America Special Paper 433*, 147–166, https://doi.org/10.1130/2007.2433(08).

Shapiro, N. M., M. H. Ritzwoller, J. C. Mareschal, and C. Jaupart (2004b). Lithospheric structure of the Canadian Shield inferred from inversion of surface-wave dispersion with thermodynamic a priori 971 constraints, *Geol. Soc. London Special Pub., 239*, 175-194, doi:110.1144/GSL.SP.2004.1239.1101.1112.

Shapiro, N. M., M. Campillo, L. Stehly, and M. H. Ritzwoller (2005). High-resolution surface-wave tomography from ambient seismic noise, *Science, 307(5715)*, 1615-1618.

Stéphane Mazzotti, Roy D. Hyndman; Yakutat collision and strain transfer across the northern Canadian Cordillera. *Geology 2002; 30 (6)*: 495–498. doi: https://doi.org/10.1130/0091-7613(2002)030<0495:YCASTA>2.0.CO;2.

Tilmann, F., Benz, H., Priestley, K., Okubo, P. (2001). P wave velocity structure of the uppermost mantle beneath Hawaii from travel time tomography. *Geophysical Journal International 146*, 594–606.

Van der Lee, S., and A. Frederiksen (2005). Surface wave tomography applied to the North American upper mantle, in Seismic Earth: *Array Analysis of Broadband Seismograms*, edited by G. Nolet, pp. 67-80, AGU Geophysical Monograph 157, Washington, DC.

Whitmeyer, S. J., & Karlstrom, K. E. (2007). Tectonic model for the Proterozoic growth of North America. *Geosphere, 3(4)*, 220–259.